Article

Developmental Cell

Histone H3 lysine 4 trimethylation in sperm is transmitted to the embryo and associated with diet-induced phenotypes in the offspring

Graphical Abstract

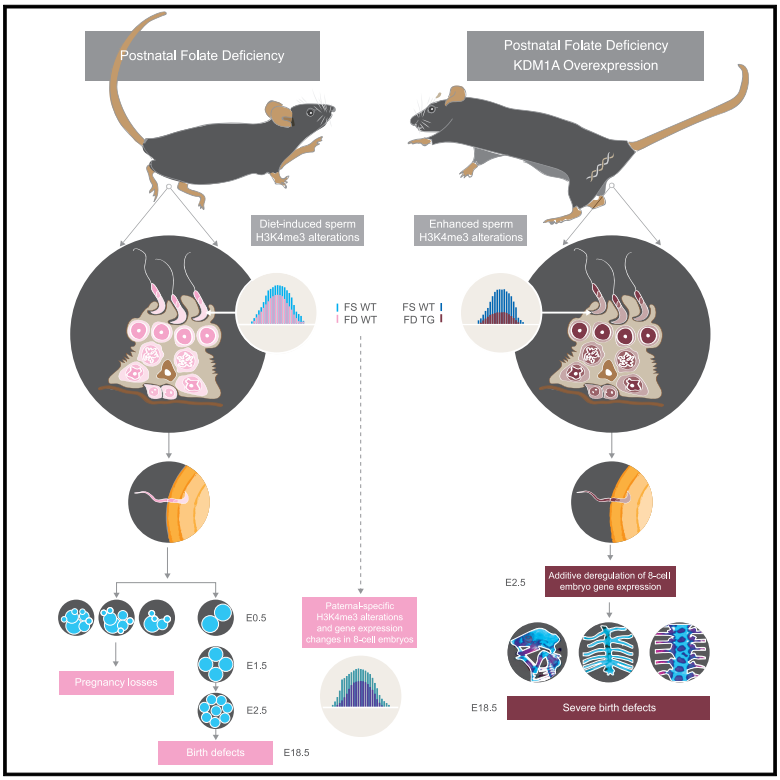

Highlights

- Postnatal paternal folate deficiency alters sperm H3K4me3 at developmental loci
- Sperm H3K4me3 aberrations are retained in the embryo & associated with birth defects
- Deregulated embryo gene expression is concordant with sperm H3K4me3 alterations
- Folate deficiency in KDM1A transgenics enhances sperm H3K4me3 levels and birth defects

Authors

Ariane Lismer, Vanessa Dumeaux, Christine Lafleur, Romain Lambrot, Julie Brind'Amour, Matthew C. Lorincz, Sarah Kimmins

Correspondence

sarah.kimmins@mcgill.ca

In Brief

Lismer et al. reveal that sperm chromatin is sensitive to dietary stress. By tracking sperm H3K4me3 in the pre-implantation embryo, they show that H3K4me3 alterations are retained and linked to deregulated gene expression. Multiple epigenetic stressors enhance sperm H3K4me3 changes and lead to increased birth defect severity in the offspring.

Lismer et al., 2021, Developmental Cell *56*, 1–16
March 8, 2021
https://doi.org/10.1016/j.devcel.2021.01.014

CellPress

Developmental Cell

CellPress

Article

Histone H3 lysine 4 trimethylation in sperm is transmitted to the embryo and associated with diet-induced phenotypes in the offspring

Ariane Lismer,[1] Vanessa Dumeaux,[2] Christine Lafleur,[3] Romain Lambrot,[3] Julie Brind'Amour,[4] Matthew C. Lorincz,[4] and Sarah Kimmins[1,3,5,*]

[1]Department of Pharmacology and Therapeutics, Faculty of Medicine, McGill University, Montreal, QC H3G 1Y6, Canada
[2]PERFORM Center, Concordia University, Montreal, QC H4B 1R6, Canada
[3]Department of Animal Science, Faculty of Agricultural and Environmental Sciences, McGill University, Montreal, QC H9X 3V9, Canada
[4]Department of Medical Genetics, Faculty of Medicine, University of British Columbia, Vancouver, BC V6T 1Z3, Canada
[5]Lead contact
*Correspondence: sarah.kimmins@mcgill.ca
https://doi.org/10.1016/j.devcel.2021.01.014

SUMMARY

A father's lifestyle impacts offspring health; yet, the underlying molecular mechanisms remain elusive. We hypothesized that a diet that changes methyl donor availability will alter the sperm and embryo epigenomes to impact embryonic gene expression and development. Here, we demonstrate that a folate-deficient (FD) diet alters histone H3 lysine 4 trimethylation (H3K4me3) in sperm at developmental genes and putative enhancers. A subset of H3K4me3 alterations in sperm are retained in the pre-implantation embryo and associated with deregulated embryonic gene expression. Using a genetic mouse model in which sires have pre-existing altered H3K4me2/3 in sperm, we show that a FD diet exacerbates alterations in sperm H3K4me3 and embryonic gene expression, leading to an increase in developmental defect severity. These findings imply that paternal H3K4me3 is transmitted to the embryo and influences gene expression and development. It further suggests that epigenetic errors can accumulate in sperm to worsen offspring developmental outcomes.

INTRODUCTION

In mammals, spermatogenesis is a highly complex cell differentiation process involving unique testis-specific gene-expression programs that are accompanied by dynamic remodeling of the chromatin (Kimmins and Sassone-Corsi, 2005; Lambrot et al., 2015; Larose et al., 2019; Maezawa et al., 2018). During this process, most histones are replaced by protamines to facilitate DNA compaction (Kimmins and Sassone-Corsi, 2005). Interestingly, 1% of sperm histones are retained in mice and 15% in men (Erkek et al., 2013; Hammoud et al., 2009). Retained histones are conserved across species from mice to men and are found at the regulatory regions of promoters implicated in spermatogenesis, sperm function, embryo development, metabolism, and routine cellular processes (Brykczynska et al., 2010; Hammoud et al., 2009; Lesch et al., 2016). Two epigenomic programs are established during spermatogenesis—the first is used for the regulation of gene expression as cells proceed from spermatogonia to sperm, and the second is postulated to serve in the establishment of gene-expression programs in the embryo (van de Werken et al., 2014).

In the developing embryo, the period of primordial germ cell migration has been suggested to be the window for developmental exposures to impact epigenomic reprogramming of the gametes (Hanson and Skinner, 2016). In men, however, sperm quality is variable throughout their lifetime and reflects their health, lifestyle, and diet (Eisenberg et al., 2014). This suggests that sperm epigenome sensitivities to exposures from environmental stressors may not be restricted to the *in utero* development period and may extend throughout life. Poor diets can induce changes to DNA methylation and non-coding RNAs in mouse sperm (Chen et al., 2016; Ly et al., 2017; Radford et al., 2014; Rodgers et al., 2013; Sharma et al., 2016; Watkins et al., 2018). However, how a micro-nutrient deficiency impacts the establishment and transmission of mammalian sperm chromatin at a genome-wide level is not known. Folate levels influence the availability of S-adenosylmethionine (SAM), the universal methyl donor for methylation reactions (Serefidou et al., 2019). A folate deficiency or supplementation interferes with the methyl-donor cycle and is linked to alterations in histone and DNA methylation levels in mouse sperm (Lambrot et al., 2013; Ly et al., 2017). Padmanabhan and colleagues conducted a seminal study showing the importance of folate metabolism in maternal epigenetic inheritance, offspring epigenetic stability, and proper development. Female mice with a mutation in *Mtrr*, a gene that participates in folate metabolism, gave rise to offspring with congenital

Please cite this article in press as: Lismer et al., Histone H3 lysine 4 trimethylation in sperm is transmitted to the embryo and associated with diet-induced phenotypes in the offspring, Developmental Cell (2021), https://doi.org/10.1016/j.devcel.2021.01.014

malformations, developmental delay, and tissue-specific loss of DNA methylation (Padmanabhan et al., 2013). We have shown that a paternal folate deficiency beginning *in utero* globally alters sperm histone methylation levels, as measured by western blotting (Lambrot et al., 2013). We attributed these changes to alterations in the folate cycle, which may have impacted the establishment of histone methylation during primordial germ cell epigenetic reprogramming (Hajkova et al., 2008; Hill et al., 2018). Whether changes in histone methylation can occur outside primordial germ cell reprogramming is unknown.

How mammalian paternal chromatin contributes to development and gene expression regulation in the embryo is not well understood. Recently, Zhang et al. concluded that sperm H3K4me3 was reprogrammed in the pronuclear stage 5 (PN5) zygote, only to be regained by the late 2-cell stage at the same genomic loci as H3K4me3 regions in sperm (Zhang et al., 2016). These findings contradict what is known about the conserved role of sperm H3K4me in regulating embryo development. A study using *Xenopus laevis* demonstrated that sperm H3K4me2/3 were enriched at promoters of genes that are expressed in the embryo, and that H3K4me2/3 establishment during spermatid to sperm transition was critical for embryonic gene expression (Teperek et al., 2016). Further confirming a role for paternal histone H3K4me in embryo development was a study conducted by Aoshima et al., wherein the authors showed that overexpressing a H3K4 lysine to methionine mutant in mouse embryos resulted in an aberrant zygotic genome activation in the paternal pronucleus (Aoshima et al., 2015). This coincided with decreased H3K4me1/3 and led to developmental arrest of H3K4 mutant overexpressing embryos (Aoshima et al., 2015). In our prior studies, we aimed to determine whether sperm H3K4me2/3 served a function in embryonic development and gene expression (Lismer et al., 2020; Siklenka et al., 2015). To do so, we generated transgenic mice that overexpressed the histone lysine demethylase KDM1A in developing sperm only. The overexpression of KDM1A during spermatogenesis led to differential H3K4me2/3 enrichment at sperm promoters, early postnatal death of offspring, and a high number of congenital anomalies in offspring (Lismer et al., 2020; Siklenka et al., 2015). Differentially enriched H3K4me2 promoters in sperm were linked to altered embryonic gene expression (Siklenka et al., 2015). Recent findings in this model revealed that H3K4me3, but not H3K4me2, was associated with transgenerational inheritance (Lismer et al., 2020). Although H3K4me3 is not a direct target of KDM1A, we attributed its alteration to compensatory mechanisms involving H3K4me3 writers, such as the histone methyltransferase MLL2, which can form a complex with KDM1A (Hyun et al., 2017). Whether alterations in sperm H3K4me3 levels are transmitted from the sperm to the pre-implantation embryo has yet to be demonstrated.

Every year, birth defects occur in 7.9 million infants worldwide, and children born in populations of low socio-economic background have an increased susceptibility toward developing a complex disease (Christianson et al., 2006; Yang et al., 2008). Although some birth defects are caused by genetic factors or infectious diseases, over half of birth defects remain idiopathic (Ingrid and Zhaurova, 2008). Worldwide micro-nutrient deficiencies, including folate deficiency, remain a persistent concern with severe health consequences for child development (Bailey et al., 2015). In at-risk communities with a significant disease burden and higher rates of birth defects, more than one environmental factor is associated with poor health (Yang et al., 2008). Increased health risk is attributed to environmental factors, such as poor qualities of diet, water, and air, as well as exposures to endocrine disruptors (World Health Organization, 2016). We hypothesized that the incidence of negative reproductive outcomes and inherited complex diseases may, in part, be attributed to changes in the sperm epigenome that can be compounded by multiple exposures.

In this study, we used wild-type (WT) or KDM1A overexpressing transgenic (TG) mice (Lismer et al., 2020; Siklenka et al., 2015) on either a postnatal folate-deficient (FD) or control folate-sufficient diet (FS) to answer the following questions: (1) Can a folate deficiency beginning at weaning alter sperm H3K4me3 enrichment?; (2) Can a previously damaged sperm epigenome, as occurs in KDM1A TG sperm, be cumulatively impacted by another epigenome modulator (folate deficiency) and lead to enhanced developmental defects in the offspring?; and (3) Do exposure-induced changes in sperm H3K4me3 enrichment persist in embryos and are they associated with abnormal embryonic gene expression and development? We demonstrate that a postnatal paternal folate deficiency is associated with birth defects in the offspring and show that altered sperm H3K4me3 is found at developmental loci that overlap genes with differential expression in the pre-implantation embryo. Intriguingly, changes in sperm H3K4me3 track to the paternal chromatin of the zygote. We further reveal that regions with altered H3K4me3 in FD sperm retain H3K4me3 aberrancies in 8-cell embryos at the same genomic loci. Feeding an FD diet to KDM1A TG mice that have pre-existing differential H3K4me3 enrichment in sperm, enhances sperm H3K4me3 alterations in comparison to WT males fed with an FD diet. These cumulative changes in sperm H3K4me3 are associated with a greater perturbation of gene expression in the embryo, as well as an increased severity in developmental abnormalities in the offspring. These findings suggest that sperm H3K4me3 contributes to environmentally influenced phenotypes in the next generation and raises the possibility that exposure to several environmental stresses can cumulatively impact the epigenome.

RESULTS

Paternal folate deficiency beginning at weaning is associated with birth defects in the offspring, and in male mice overexpressing KDM1A is linked to enhanced phenotype severity

We fed WT or KDM1A transgenic (TG) C57BL/6J males with a FS, (2.0 mg/kg) or FD, (0.3 mg/kg) diet post weaning beginning at 3 weeks of age (Figure 1A). After 9–11 weeks of dietary exposure spanning over two cycles of spermatogenesis, males were bred to WT female C57BL/6J mice fed with a regular mouse chow diet (Figure 1A). Pregnancy outcomes were assessed on embryonic day E18.5 (Figures S1A and S1B). TG males fed with an FD diet sired litters with significantly higher variability in pre-implantation loss compared with WT males fed with an FS diet (F test, $p < 0.05$; Figure S1A). Post-implantation losses showed an increased variability in both litters sired by FD WT

Please cite this article in press as: Lismer et al., Histone H3 lysine 4 trimethylation in sperm is transmitted to the embryo and associated with diet-induced phenotypes in the offspring, Developmental Cell (2021), https://doi.org/10.1016/j.devcel.2021.01.014

CellPress

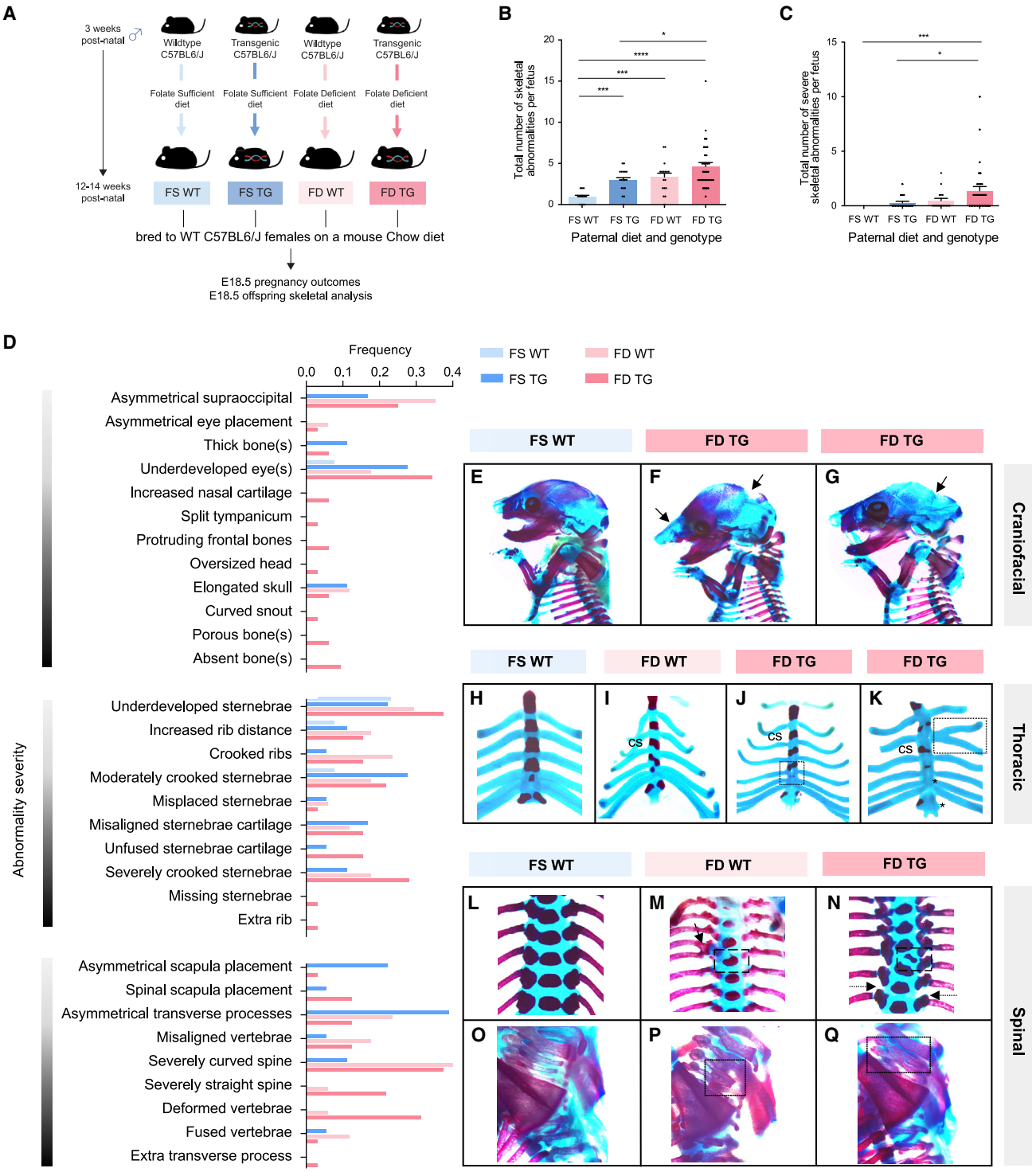

Figure 1. Paternal folate deficiency beginning at weaning is associated with birth defects in the offspring, and in male mice overexpressing KDM1A is linked to enhanced phenotype birth defect severity

(A) Skeletal analysis was performed on E18.5 offspring of wild-type C57BL6/J (WT) or KDM1A transgenic C57BL6/J (TG) males fed with an FS, (2.0 mg/kg) or FD, (0.3 mg/kg) diet and bred to WT C57BL6/J females on a mouse chow diet. Fetuses were stained in Alcian blue for cartilage and Alizarin red for bone.

(B) Number of total skeletal abnormalities per E18.5 fetus. Statistical tests for total number of abnormalities per fetus: Mann-Whitney's U-test, Holm-Bonferroni corrected (*$p < 0.05$, ***$p < 0.001$, ****$p < 0.0001$).

(legend continued on next page)

Please cite this article in press as: Lismer et al., Histone H3 lysine 4 trimethylation in sperm is transmitted to the embryo and associated with diet-induced phenotypes in the offspring, Developmental Cell (2021), https://doi.org/10.1016/j.devcel.2021.01.014

and FD TG males compared with litters sired by FS WT males (F test, $p < 0.05$ for both comparisons; Figure S1B).

Skeletal analysis was used for in-depth characterization of birth defects in E18.5 offspring of WT or TG males fed with either an FS or FD diet (Figures 1B–1Q). This analysis revealed a spectrum of abnormalities in offspring sired by FD WT, FS TG, and FD TG males (Mann-Whitney's U-test, $p < 0.001$ for FS WT versus FS TG and FS WT versus FD WT, $p < 0.0001$ for FS WT versus FD TG, $p < 0.05$ for FS TG versus FD TG; Figures 1B–1Q and S1C). Malformations included crooked sternebrae and unfused sternebrae cartilage, asymmetrical bones, and bent ribs (Figures 1D, 1I, 1J, and 1K). The fetuses sired by the FD TG males had the most severe birth defects (Mann-Whitney's U-test, $p < 0.001$ for FS WT versus FD TG, $p < 0.05$ for FS TG versus FD TG; Figures 1C, 1D, 1F, 1G, 1J, 1K, 1N, 1Q, and S1C). These severe abnormalities ranged from craniofacial defects, such as missing bones and under-ossified skulls (Figures 1F and 1G), to spinal defects, such as deformed or misplaced vertebrae and extra transverse processes (Figures 1N and 1Q). This analysis shows that similar to a lifetime paternal folate deficiency beginning *in utero* (Lambrot et al., 2013), a paternal folate deficiency beginning *postnatally* is also associated with skeletal defects and pregnancy loss. Furthermore, our analysis demonstrates that feeding the FD diet to TG sires with an already altered sperm epigenome is accompanied by augmented birth defect severity in the next generation.

Folate deficiency beginning at weaning alters H3K4me3 levels at specific genomic loci in WT sperm

We next aimed to understand if there were diet-induced alterations in sperm H3K4me3 that could be associated with the birth defects observed in E18.5 offspring. To do so, we generated high-quality sperm H3K4me3 ChIP-seq libraries for each experimental group (n = 5 per group; Figure S2). On an average, 97% of the reads aligned to the mouse genome, yielding approximately 35 million reads per sperm sample, of which 24 million mapped uniquely (Table S1). We normalized counts in H3K4me3-enriched regions to correct for library size, composition bias, and batch effects and obtained a correlation of over 0.98 between replicates (Figure S2B). Comparing our data to existing published datasets for ChIP-seq on H3K4me3 in sperm indicates that our experimental approach yielded a superior signal at regions with both broad and narrow peaks (Figure S3; Table S1) (Erkek et al., 2013; Jung et al., 2017; Zhang et al., 2016). The increased quality and sequencing depth of our datasets improved our ability to detect enrichment differences in sperm H3K4me3.

To determine whether sperm chromatin is sensitive to low dietary folate beginning at weaning, we first compared our H3K4me3 datasets from FS WT and FD WT sperm (Figure 2). Principal component analysis of normalized H3K4me3 marked regions in sperm revealed a clear segregation of H3K4me3 enrichment levels on principal component 1 (PC1), with diet being the major source of variability (Figure 2A, PERMANOVA, permutation-based $p < 0.01$; n = 1,000 permutations). To capture the regions that were the most altered by folate deficiency, we focused our analysis on the top 5% of genomic regions impacted by diet (PC1) and determined directionality changes of H3K4me3 enrichment in FD WT sperm (Figure 2B). Of the 1,434 selected regions, 650 had increased H3K4me3 (t test, $p < 0.05$; Figures 2Biii, 2C, and 2E) and 784 had decreased H3K4me3 in FD WT sperm (t test, $p < 0.0001$; Figures 2Biv, 2D, and 2E). Interestingly, regions with increased and decreased H3K4me3 had different genomic location distributions (Fisher test, $p < 0.001$, Figures 2F and 2G). Whereas regions with increased H3K4me3 were predominantly located less than 1 kb from annotated transcriptional start sites (TSS, Fisher test, $p < 0.0001$; Figure 2F), regions with decreased H3K4me3 were primarily found over 10 kb away from the TSS in intergenic regions (Fisher test, $p < 0.0001$; Figure 2G). Certain studies suggest that sperm histones are mostly retained at CpG-rich sequences that lack DNA methylation (Erkek et al., 2013), whereas others report that histones are mainly found in distal intergenic regions with low CpG density (Carone et al., 2014; Yamaguchi et al., 2018). Our ChIP-seq datasets show that H3K4me3 is found at both regions of low and high CpG density (Figures S4A–S4D). We defined regions of high or low H3K4me3 enrichment and high or low CpG density using the local minima of their respective density curves (CpG density threshold = 0.478; Figures S4A and S4D). Sites with increased H3K4me3 showed a preferential enrichment for regions of high CpG density (hypergeometric test, $p < 0.0001$), whereas those with decreased H3K4me3 were more associated to areas of low CpG density (hypergeometric test, $p < 0.0001$; Figure S4B). All regions altered by the folate deficiency were found at regions with low or moderate levels of H3K4me3, and regions with the highest enrichment for H3K4me3 were unaltered by diet (Figure S4B). Taken together, our analysis shows that the chromatin landscape in sperm is sensitive to a folate deficiency outside of primordial germ cell epigenetic reprogramming, and that regions with increased or decreased H3K4me3 in FD WT sperm occur at distinct genomic loci.

Regions of the sperm epigenome sensitive to low dietary folate include promoters and putative enhancers with functional implications for development

To gain functional insight with regards to diet-affected regions with altered H3K4me3 in FD WT sperm, we performed a gene

(C) Number of severe skeletal abnormalities per E18.5 fetus. Statistical test for number of severe abnormalities per fetus: Mann-Whitney's U-test, Holm-Bonferroni corrected (*$p < 0.05$, ***$p < 0.001$). For (B and C), each dot on the box plot corresponds to an individual E18.5 fetus. We analyzed 12 fetuses from FS WT males, 18 from FS TG males, 19 from FD WT males, and 32 from FD TG males. 3–6 males were used and 7–13 litters were generated per group.

(D) The frequency of craniofacial, thoracic, and spinal abnormalities in E18.5 fetuses from described breeding. The severity of abnormality is shown by color gradient.

(E–G) Craniofacial abnormalities in FD TG offspring, including missing nasal bones, porous bones (F and G, black arrow), as well as elongated skull (G).

(H–K) Thoracic abnormalities in FD WT and FD TG offspring involving crooked sternebrae (I, J, K, cs). Offspring from FD TG males with unfused sternebrae cartilage, abnormally fused rib cartilage (J and K, black box), and missing sternebrae bones (K, star).

(L–Q) Spinal abnormalities in offspring from WT and TG males fed with an FD diet. In the trunk area, abnormalities, including extra ribs (M, dashed arrow), abnormal thoracic centers of ossification (M and N, dashed box), and asymmetrical placement of transverse processes (N, dotted arrow). In the cervical area, FD WT and FD TG offspring with fused vertebrae (P and Q, dotted box).

Please cite this article in press as: Lismer et al., Histone H3 lysine 4 trimethylation in sperm is transmitted to the embryo and associated with diet-induced phenotypes in the offspring, Developmental Cell (2021), https://doi.org/10.1016/j.devcel.2021.01.014

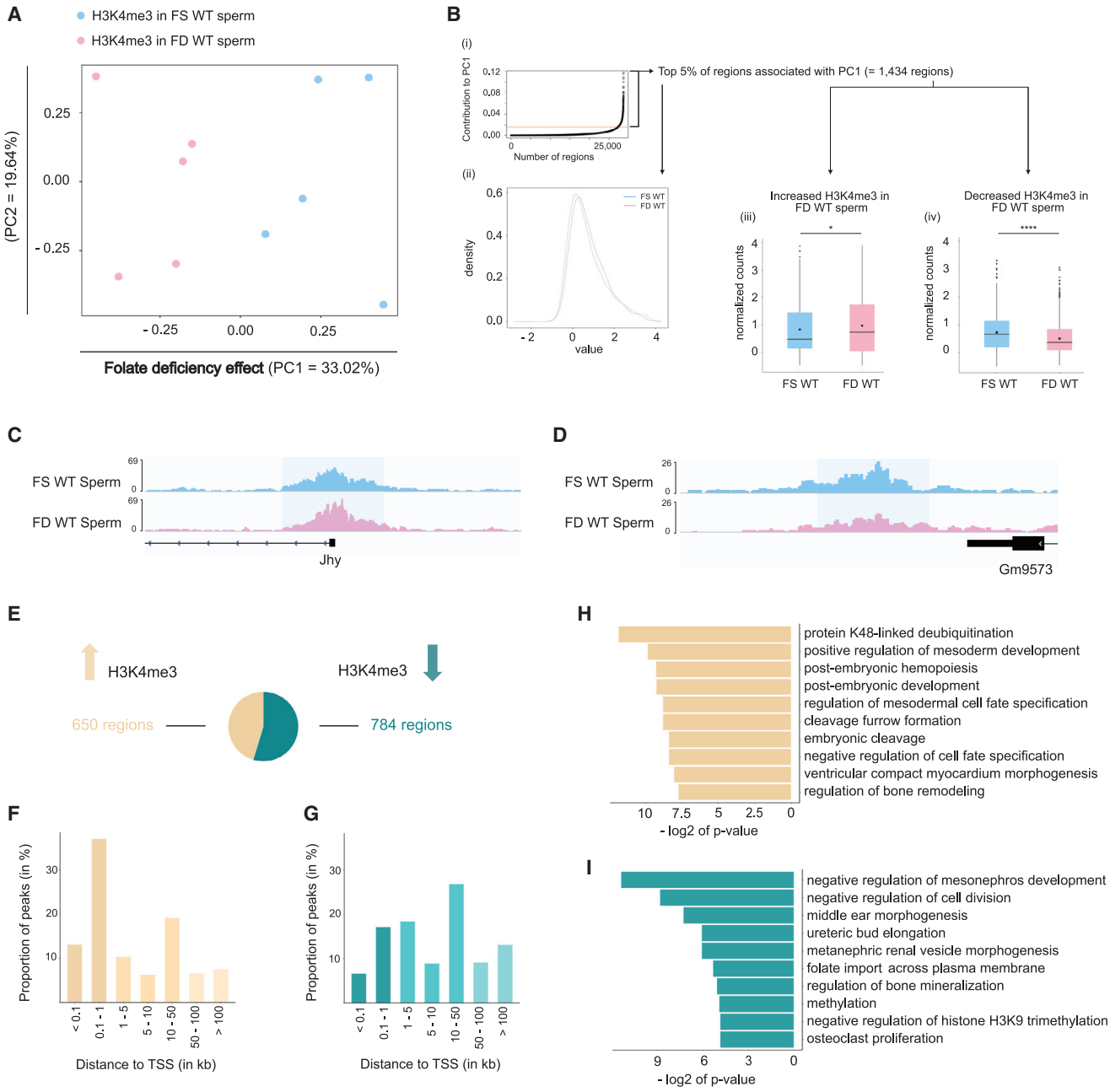

Figure 2. Folate deficiency beginning at weaning alters H3K4me3 levels in WT sperm at developmental loci

ChIP-sequencing for H3K4me3 was performed on the sperm of C57BL6/J WT males fed with an FS or FD diet beginning at weaning (n = 5 males per group).

(A) Principal component analysis on normalized counts enriched in H3K4me3 (= 28,679 regions) for FS WT and FD WT sperm.

(B) Selection of the top 5% of regions contributing to principal component 1 (PC1, PERMANOVA, permutation based, $p < 0.01$, n = 1,000 permutations) (Bi), and density distribution of normalized counts for these regions (Bii). Grouping of selected regions based on directionality changes of H3K4me3 levels and boxplots of regions with increased (t test, *$p < 0.05$) (Biii) and decreased (t test, ****$p < 0.0001$) (Biv) H3K4me3 levels in FD WT sperm. Black line on boxplots correspond to the median, black dot corresponds to the mean.

(C and D) Integrative Viewer Genome tracks of (C) the *Jhy* promoter with increased H3K4me3 in FD WT sperm and (D) a putative mouse embryonic stem cell enhancer (Shen et al., 2012) with decreased H3K4me3 in FD WT sperm.

(E) Pie chart indicating number of regions with increased H3K4me3 (= 650 regions) versus decreased H3K4me3 (= 784 regions) in FD WT sperm.

(F) Distribution of regions with increased H3K4me3 levels in FD WT sperm relative to the TSS.

(G) Distribution of regions with decreased H3K4me3 levels in FD WT sperm relative to the TSS.

(H) Selected significant pathways from gene ontology analysis on the promoters (= 270) with increased H3K4me3 in FD WT sperm.

(I) Selected significant pathways from gene ontology analysis on the promoters (= 130) with decreased in FD WT sperm. Full list of gene ontology pathways provided in Table S2.

Please cite this article in press as: Lismer et al., Histone H3 lysine 4 trimethylation in sperm is transmitted to the embryo and associated with diet-induced phenotypes in the offspring, Developmental Cell (2021), https://doi.org/10.1016/j.devcel.2021.01.014

ontology enrichment analysis on the promoters of these regions (Figures 2H and 2I, full list of gene ontology pathways provided in Table S2). Promoters with increased H3K4me3 (= 270) were enriched for genes involved in early pre- and post-implantation embryogenesis, bone remodeling, and heart development (Figure 2H). Promoters with decreased H3K4me3 (= 130) were enriched for genes involved in osteoclast proliferation, kidney and ear development, and chromatin remodeling (Figure 2I). These results suggest an overall vulnerability of developmental genes to the paternal folate deficiency. We note that genes involved in folic acid transport were significantly enriched in promoters with decreased H3K4me3 in FD WT sperm, implying a direct biological response to the folate deficiency. Gene ontology enrichment analysis on promoters unaffected by diet (= 1,542 promoters out of 4,034 regions), revealed multiple pathways involved in spermatogenesis and fertilization (Figures S4B and S4C). This analysis is in line with our previous findings, wherein males on an FD diet beginning *in utero* and throughout adulthood, have normal testes morphology, sperm counts, and fertilization abilities (Lambrot et al., 2013).

As a high H3K4me1 to H3K4me3 ratio is suggestive of enhancer function (Calo and Wysocka, 2013), H3K4me imbalances induced by H3K4me3 alterations in sperm may compromise developmental enhancer functions in the embryo. Because regions with altered H3K4me3 in FD WT sperm were present in the intergenic space, we intersected regions with increased or decreased H3K4me3 to putative tissue-specific enhancer annotations (Attanasio et al., 2013; Shen et al., 2012) (Figures S4E–S4H). Notably, regions with decreased H3K4me3 in FD WT sperm had more than four times the number of over-represented classes of putative enhancers compared with regions with increased H3K4me3 (Figures S4F and S4H). Testes, craniofacial, limb and placenta enhancers were among the over-represented classes of putative enhancers for differentially enriched H3K4me3 regions (Figures S4G and S4H), and this occurred more frequently than expected by chance (permutation-based, $p < 0.05$, n = 1,000 permutations; Figure S4H). Overall, affected enhancer and promoter classes reflect the phenotypes observed in the E18.5 offspring from FD WT males, which included eye abnormalities and asymmetrical skull bones (Figure 1D).

Folate deficiency is associated with exacerbated H3K4me3 changes in the sperm of KDM1A TG males

We were interested to know whether the increase in severity of phenotypes in E18.5 embryos sired by FD TG males were associated with exacerbated H3K4me3 alterations in FD TG sperm. First, we identified regions with altered H3K4me3 between FS WT and FD TG sperm (Figures 3A–3D), then we assessed H3K4me3 enrichments at these regions across all experimental groups (Figures 3E–3K). Principal component analysis on normalized H3K4me3 regions between FS WT and FD TG sperm showed a clear segregation between the two groups on PC1 (PERMANOVA, permutation-based $p < 0.01$; n = 1,000 permutations). This segregation was more visible in comparison to the principal component analysis for FS WT and FD WT sperm (Figures 2A and 3A). We selected the top 5% most impacted regions that were associated with PC1 showing the diet and genotype effects. Our analysis identified 483 and 951 regions with increased (t test; FDR < 0.05; Figure 3E) and decreased (t test; FDR < 0.0001; Figure 3G) H3K4me3, respectively. Promoters with increased H3K4me3 in FD TG sperm (= 84) were enriched in genes involved in synaptic and cell development (Figure 3C, full list of gene ontology pathways provided in Table S2). Interestingly, promoters with decreased H3K4me3 in FD TG sperm (= 341) were enriched in genes involved in processes that reflected the E18.5 skeletal phenotype in FD TG offspring (Figures 3D and 1). These pathways included cartilage formation, bone mineralization, neural crest cell migration, pattern formation, axis specification, and craniofacial development (Figure 3D, full list of gene ontology pathways provided in Table S2). We next assessed the level of H3K4me3 enrichment at regions with altered H3K4me3 in FD TG sperm across all experimental groups to determine if the folate deficiency coupled to the KDM1A overexpression exacerbated changes in H3K4me3 in sperm (Figures 3E–3K). For regions with increased H3K4me3 in FD TG sperm, the H3K4me3 levels in FS TG and FD WT sperm were not significantly altered compared with FS WT or FD TG sperm (Figures 3E and 3F). Conversely, regions with decreased H3K4me3 were lower in FS TG and FD WT sperm compared with FS WT sperm (t test, FDR < 0.001 and FDR < 0.01, respectively; Figures 3G–3K). Strikingly, these regions were the lowest in FD TG sperm (t test, FDR < 0.0001 for FS WT versus FD TG, FS TG versus FD TG, and FD WT versus FD TG; Figures 3G–3K). Our analysis shows that feeding an FD diet to KDM1A TG males that have pre-existing H3K4me3 alterations in sperm, leads to an enhanced reduction of H3K4me3 in comparison to FD WT and FS TG sperm. This outcome suggests that when there are pre-existing changes to H3K4me3 in sperm, they can be cumulatively altered when exposed to another epigenome modifying factor, in this case folate deficiency.

8-cell embryos from FD WT males have aberrant gene expression that overlap promoters with altered H3K4me3 in FD WT sperm

To delineate how a paternal folate deficiency and KDM1A overexpression alters gene expression in the pre-implantation embryo, we focused on the 8-cell stage, after zygotic genome activation, and when the embryo is synthesizing its own mRNA to direct development. We probed the 8-cell stage as in the earlier 2-cell stage the vast majority of RNA present, known as the dormant mRNA, originates from the oocyte (Schultz et al., 2018). We bred WT or TG males fed with an FS or FD diet to WT females fed with an FS diet and collected embryos for developmental assessment (Figure S5A). The percentage of abnormal embryos with disrupted cleavage patterns and inconsistent cell size increased in litters sired by FD TG males (t test, $p < 0.05$; Figure S5B). Morphologically normal 8-cell embryos were collected on embryonic day E2.5, as we were interested in the transcriptome of embryos that would likely have implanted and survived to term. We rationalized that the normal embryos would be more likely to have altered transcription of genes that corresponded to the fetal abnormalities observed (Figure 1). Multidimensional scaling visualization of normalized expressed transcripts revealed clear clustering of embryos based on paternal diet and genotype (Figure S5C). We identified 3,263 transcripts with altered expression in 8-cell embryos from FD WT males compared with 8-cell embryos from FS WT males, comprising 1,946 transcripts with increased expression and

Please cite this article in press as: Lismer et al., Histone H3 lysine 4 trimethylation in sperm is transmitted to the embryo and associated with diet-induced phenotypes in the offspring, Developmental Cell (2021), https://doi.org/10.1016/j.devcel.2021.01.014

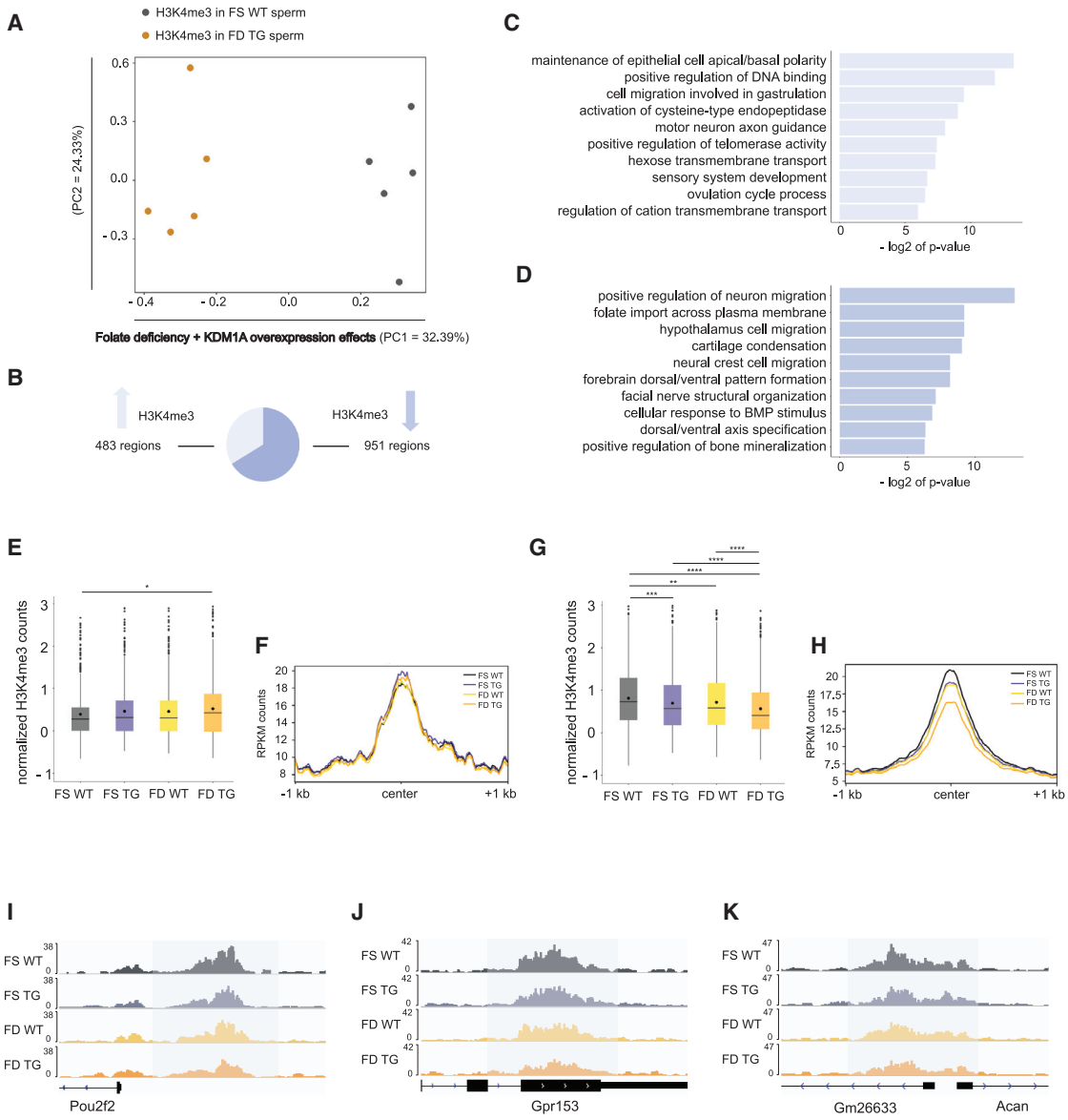

Figure 3. Folate deficiency exacerbates H3K4me3 changes in the sperm of KDM1A TG males

ChIP-sequencing for H3K4me3 was performed on the sperm of C57BL6/J WT or C57BL6/J TG males fed with an FS or FD diet beginning at weaning (n = 5 males per group).

(A) Principal component analysis on normalized counts enriched in H3K4me3 (= 28,679 regions) for FS WT and FD TG sperm.

(B) Selection of the top 5% of regions contributing to principal component 1 (PC1, PERMANOVA, permutation-based, $p < 0.01$, n = 1,000 permutations) and distribution of regions with increased H3K4me3 (= 483 regions) and regions with decreased H3K4me3 (= 951 regions) in FD TG sperm compared with FS WT sperm.

(C) Selected significant pathways from gene ontology analysis on the promoters (= 84) with increased H3K4me3 in FD TG sperm.

(D) Selected significant pathways from gene ontology analysis on the promoters (= 341) with decreased H3K4me3 in FD TG sperm.

(E–H) (E and G) Boxplots of $\log_2$ normalized H3K4me3 counts for regions with increased (t test, *FDR < 0.05 for FS WT versus FD TG) (E) and decreased (t test, ***FDR < 0.001 for FS WT versus FS TG, **FDR < 0.01 for FS WT versus FD WT, ****FDR < 0.0001 for FS WT versus FD TG, FS TG versus FD TG, FD WT versus FD TG) (G) H3K4me3 in FD TG sperm across all experimental groups. Black line on boxplots correspond to the median, black dot corresponds to the mean. (F and H) Profile plots of RPKM normalized H3K4me3 counts ± 1 kb from the center of the regions with increased (F) or decreased (H) H3K4me3 across all experimental groups.

(I–K) Integrative genome viewer tracks of the *Pou2f2* (I), *Gpr153* (J), and *Acan* (K) genes with cumulative decrease of H3K4me3 in FS WT, FS TG, FD WT, and FD TG sperm.

Please cite this article in press as: Lismer et al., Histone H3 lysine 4 trimethylation in sperm is transmitted to the embryo and associated with diet-induced phenotypes in the offspring, Developmental Cell (2021), https://doi.org/10.1016/j.devcel.2021.01.014

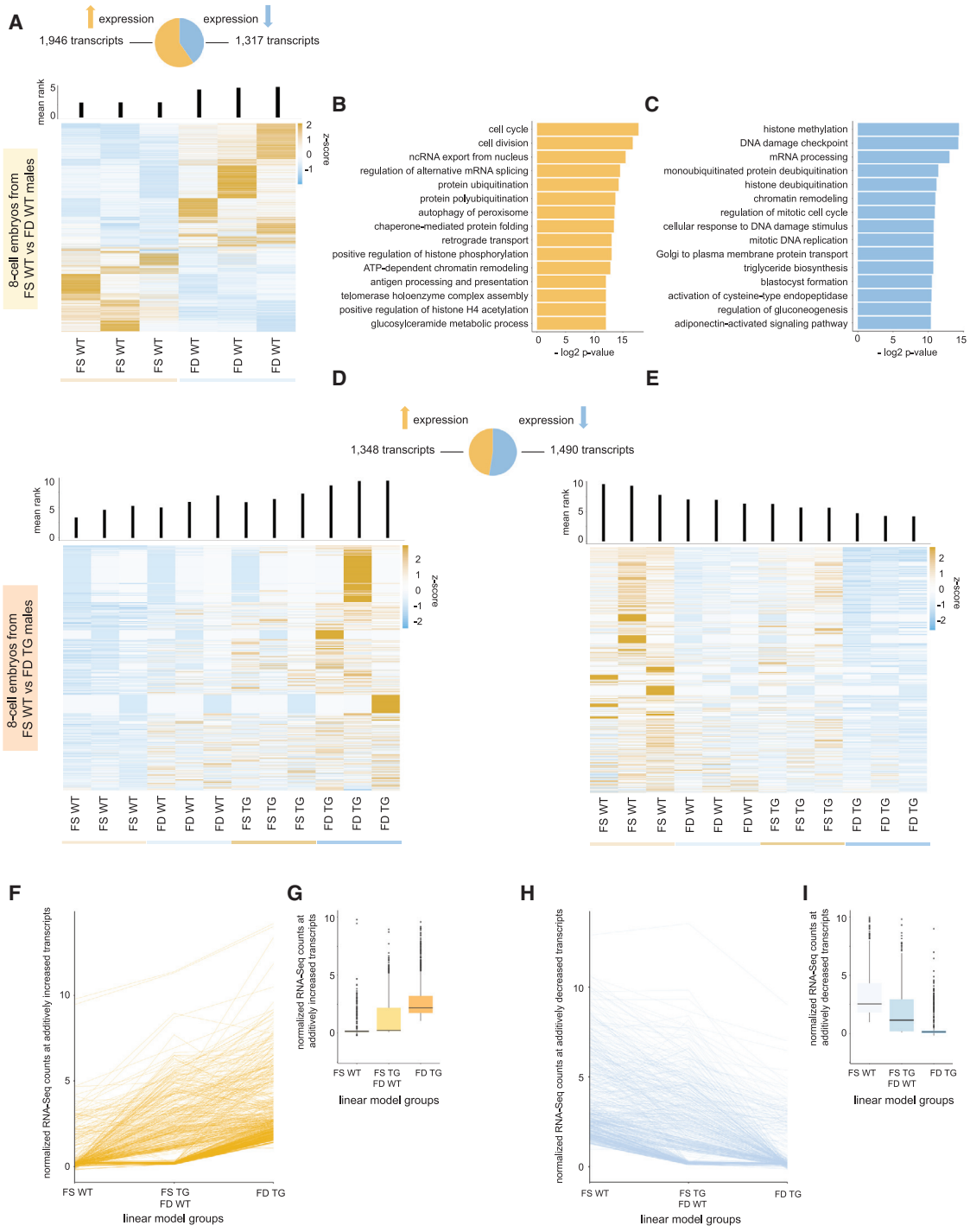

Figure 4. Paternal folate deficiency is associated with deregulated gene expression in the pre-implantation embryo.

Low-input mRNA-Sequencing was performed on 8-cell embryos from C57BL6/J WT or TG males fed with an FS or FD deficient diet and bred to C57BL6/J FS WT females (n = 3 per group with approximatively 14 embryos pooled per replicate. A different male was used for each replicate; Figure S5A).

(A) Heatmap of normalized transcripts with altered expression in 8-cell embryos from FS WT versus FD WT males (3,263 differentially expressed transcripts, FDR < 0.1) and directionality changes. The mean transcript rank provides an estimate of how extreme the expression over all transcripts is in each sample compared with the other samples.

(B) Selected significant pathways from gene ontology analysis on promoters of transcripts with increased expression in 8-cell embryos from FD WT males (= 1,693 unique promoters).

(C) Selected significant pathways from gene ontology analysis on promoters of transcripts with decreased expression in 8-cell embryos from FD WT males (= 1,182 unique promoters). Full list of gene ontology pathways provided in Table S2.

(legend continued on next page)

Please cite this article in press as: Lismer et al., Histone H3 lysine 4 trimethylation in sperm is transmitted to the embryo and associated with diet-induced phenotypes in the offspring, Developmental Cell (2021), https://doi.org/10.1016/j.devcel.2021.01.014

1,317 transcripts with decreased expression (FDR < 0.1, Figure 4A). A number of key regulator genes in chromatin remodeling during pre-implantation development, such as *Dnmt1*, *Hdac6*, *Dnmt3b*, *Kdm3a*, *Wdr5*, and *Tet2*, were impacted (Chen and Dent, 2014; Eckersley-Maslin et al., 2018). Altered transcripts were enriched for genes involved in fundamental pathways of pre-implantation development (= 2,391 unique genes mapped to 3,263 significant transcripts; Figures 2B and 2C, full list of gene ontology pathways provided in Table S2). Transcripts with increased expression were involved in cell cycle, cell division, and histone modification (= 1,693 unique genes; Figure 2B). Transcripts with decreased expression were heavily implicated in chromatin remodeling and embryonic development (= 1,182 unique genes; Figure 2C).

We then determined whether H3K4me3 alterations in sperm were associated with changes in 8-cell embryo gene expression. Remarkably, 25% of promoters with altered H3K4me3 in FD WT sperm that mapped to genes expressed in the 8-cell embryo also corresponded to differentially expressed genes in 8-cell embryos sired by FD WT males (Fisher test, $p < 0.0001$; Figure S5G). For promoters with increased H3K4me3 in sperm there was a significant correspondence with increased gene expression in the embryo (Fisher test, $p < 0.01$; Figure S5H). As expected, since regions with decreased H3K4me3 in FD WT sperm were predominantly found in intergenic space, we did not find significant overlap between decreased H3K4me3 in sperm and decreased gene expression in the embryo (Figures S5I and 2G). This modest yet significant correspondence between sperm H3K4me3 alterations and differentially expressed genes in the embryo lends support to the idea that paternal H3K4me3 may, in part, instruct gene expression in the pre-implantation embryo.

Paternal folate deficiency combined with the KDM1A overexpression additively impact the 8-cell embryo transcriptome

Our prior analyses revealed that in sperm, H3K4me3 alterations were significantly enhanced in TG sires fed with an FD diet at regions that reflected the phenotypes in E18.5 progeny (Figures 1 and 3). Taken together with the increased severity of skeletal abnormalities in offspring from FD TG males, this implies that there can be additive effects of epigenetic stressors on sperm chromatin that may have consequences for offspring development. Similar to our analyses in sperm, we first identified transcripts that were differentially regulated in embryos from FD TG males compared with FS WT males, to capture alterations resulting from both FD diet and pre-existing alterations in sperm H3K4me3. Next, we assessed their expression levels across all experimental groups. Our analysis identified 1,348 overexpressed transcripts and 1,490 underexpressed transcripts in FD TG compared with FS WT embryos (FDR < 0.1, 1,190 and 1,314 unique genes, respectively; Figures 4D and 4E). Differentially expressed transcripts in embryos from FD TG males significantly overlapped differentially expressed transcripts in embryos from FD WT males (Fisher test, $p < 0.0001$; Figures S5D–S5F). We observed a significant trend in change of expression for 55% of overexpressed and 46% of underexpressed transcripts with intermediate levels of expression in embryos from FS TG or FD WT and more extreme changes in embryos from FD TG males (Figures 4F–4I, test for trend FDR < 0.1).

Genes expressed in 8-cell embryos and that corresponded to promoters bearing altered H3K4me3 in FD TG sperm significantly overlapped genes with deregulated expression in embryos from FD TG males (Fisher test, $p < 0.01$; Figure S5J). However, the direction of change in H3K4me3 enrichment in the sperm did not correlate with whether the corresponding gene was up- or downregulated in the embryo (Figures S5K and S5L). This may be, in part, related to the high number of morphologically abnormal 8-cell embryos from FD TG males that were not selected for a transcriptome analysis (Figure S5B).

Paternally inherited H3K4me3 persists in pre-implantation embryo at regions with diet-altered H3K4me3 in sperm

Given that sires fed with an FD diet had altered H3K4me3 at genomic regions that corresponded with deregulated embryonic gene expression (Figures S5G–S5L), the next logical step was to determine if H3K4me3 profiles in embryos were similar to those in sperm (Figure 5). We used an existing 2-cell embryo H3K4me3 ChIP-seq data set from Liu et al. (2016), and compared 2-cell H3K4me3 regions to those in sperm (Figure 5A). This comparison revealed that 73% of regions with H3K4me3 in sperm had detectable H3K4me3 enrichment in the 2-cell embryo (Figure 5A). While this suggests that sperm may transmit H3K4me3 signatures that are retained in the embryo, we sought further confirmation that this might be the case. A study from Zhang et al. (2016) used a mouse breeding scheme (C57BL6/N female x PWK/PhJ male) that permits the assignment of ChIP-seq reads to either the maternal or paternal alleles and reported a near complete reprogramming of H3K4me3 on the paternal allele of the pre-implantation embryo. Conversely, by re-analyzing their datasets (see STAR methods), we demonstrate that the paternal allele retains significant H3K4me3 in the pre-implantation embryo, genome wide (Figures 5B–5I). We intersected our re-analyzed Zhang et al. (2016) paternal allele-specific PN5 H3K4me3 ChIP-seq data to our sperm H3K4me3 data and identified 10,693 regions of H3K4me3 overlap (Figure 5B). Remarkably, these enrichments of H3K4me3 on the paternal allele of the pre-implantation embryo persisted throughout development to the inner cell mass of the blastocyst (Figures 5C–5G).

(D and E) Heatmap of normalized transcripts with increased (1,348 transcripts, FDR < 0.1) (D) or decreased (1,490 transcripts, FDR < 0.1) (E) expression in 8-cell embryos from FS WT versus FD TG males. Samples are ordered by experimental groups.

(F–I) Transcripts with altered levels in 8-cell embryos from FD TG males were tested for significant trends in expression across experimental groups (FS WT = 1; FS TG or FD WT = 2; FD TG = 3; FDR < 0.1).

(F–I) Transcripts that were either increased (F and G, 745 transcripts) or decreased (H and I, 680 transcripts) in 8-cell embryos from FS WT versus FD TG males and with significant trends in expression across experimental groups as defined above.

(F and H) Individual lines represent the expression of each transcript averaged within each experimental group.

(G and I) Boxplots illustrating the distribution of transcript expression within each group from the linear model.

Please cite this article in press as: Lismer et al., Histone H3 lysine 4 trimethylation in sperm is transmitted to the embryo and associated with diet-induced phenotypes in the offspring, Developmental Cell (2021), https://doi.org/10.1016/j.devcel.2021.01.014

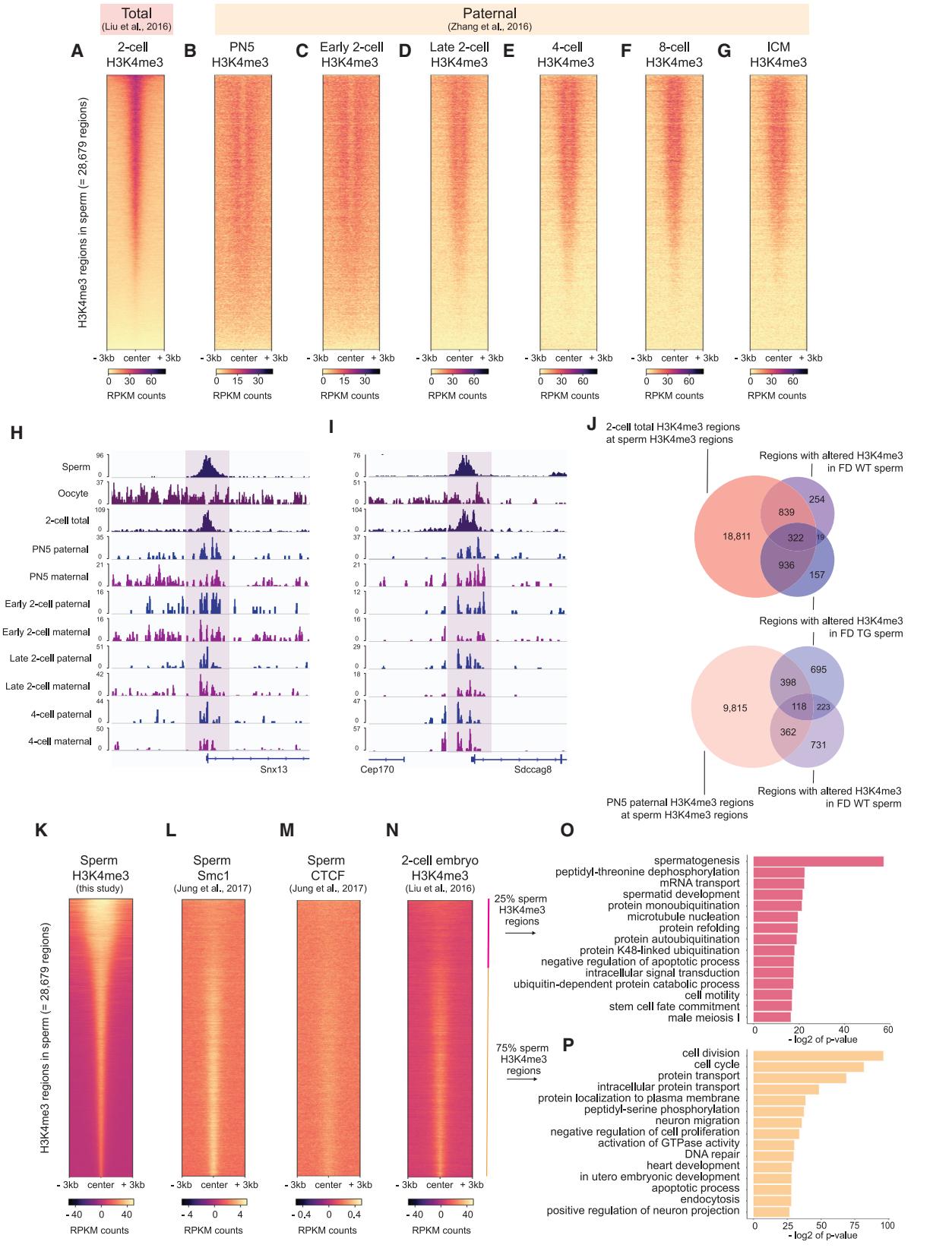

(legend on next page)

Please cite this article in press as: Lismer et al., Histone H3 lysine 4 trimethylation in sperm is transmitted to the embryo and associated with diet-induced phenotypes in the offspring, Developmental Cell (2021), https://doi.org/10.1016/j.devcel.2021.01.014

The following question we asked was whether diet sensitive H3K4me3 regions in sperm are present on the paternal allele in the pre-implantation embryo, as this would suggest a direct route for epigenetic inheritance through the paternal germline. Of the regions bearing H3K4me3 in the total 2-cell embryo (data from Liu et al., 2016), 1,161 overlapped with regions of differentially enriched H3K4me3 in the sperm of FD WT sires (Figure 5J). Similarly, 1,258 regions with H3K4me3 in the 2-cell embryo overlapped regions with altered H3K4me3 in FD TG sperm (Figure 5J). When focusing on the paternal allele H3K4me3 regions in the PN5 embryo (data from Zhang et al., 2016), 480 regions overlapped those that were differentially enriched H3K4me3 in the sperm of FD WT sires and 516 with H3K4me3 regions altered in FD TG sperm (Figure 5J). Overall, this analysis suggests that paternally inherited H3K4me3 is retained in the pre-implantation embryo and regions affected by low dietary folate in sperm co-localize to regions with H3K4me3 on the paternal allele of the PN5 embryo.

We subsequently wanted to understand what factors could be involved in the retention of sperm H3K4me3 in the embryo and embryonic gene expression. To this end, we compared FS WT sperm (data from this study) and 2-cell embryo H3K4me3 signals (data from Liu et al., 2016) to sperm-binding sites for the transcription factor CTCF and Smc1, a subunit of CTCF's interaction partner, cohesin (data from Jung et al., 2017; Figures 5K–5P). In somatic cells, CTCF and cohesin act together to facilitate chromatin interactions at distal regulatory sites and at promoters (Phillips and Corces, 2009). We found that signals for Smc1, CTCF, and H3K4me3 in sperm co-localized with H3K4me3 enriched regions in 2-cell embryos (Figures 5K and 5N). Broad H3K4me3 regions in sperm, visualized in the upper quarter of the heatmap (Figure 5K) were not enriched for Smc1 or CTCF in sperm, nor for H3K4me3 in 2-cell embryos (Figures 5K–5N). Conversely, sperm regions represented in the lower 75% of the heatmap with narrower H3K4me3 signals, co-localized with Smc1 and CTCF in sperm, as well as H3K4me3 in 2-cell embryos (Figures 5K–5N). This is consistent with the role of CTCF in preventing H3K4me3 spreading in somatic cells (Khoury et al., 2020). Top significant processes from the upper 25% of sperm H3K4me3 regions were enriched for spermatogenic events, including meiosis, spermatid differentiation, and cell motility (= 7,170 regions comprising 3,816 promoters; Figure 5O). Promoters belonging to the lower 75% of sperm H3K4me3 regions (= 21,509 regions comprising 9,682 promoters) showed mostly an enrichment for cellular processes but also included embryonic development (Figure 5P). This analysis proposes that regions with broad H3K4me3 signals in sperm, principally involved in spermatogenic processes, are reprogrammed in the pre-implantation embryo. In contrast, regions in sperm with narrow H3K4me3 signals that overlap sperm Smc1, CTCF, and 2-cell embryo H3K4me3, hint at the possibility that cohesin and CTCF may be involved in protecting those developmental H3K4me3 regions from reprogramming in the embryo and serve in pre-implantation embryo gene expression.

Paternal folate deficiency is linked to altered H3K4 trimethylation profiles in the pre-implantation embryo

To explore the potentiality that sperm H3K4me3 is transmitted and persists in the embryo to influence gene expression, we performed ultra-low-input ChIP-seq (ULI-ChIP, read statistics provided in Table S1) (Brind'Amour et al., 2015) on 8-cell embryos sired by either FS WT or FD WT males that were bred to FS WT females (Figure S6A). We compared H3K4me3 enrichment in 8-cell embryo regions to those in sperm, the oocyte, and 2-cell embryos (Figures 6A–6F). Strikingly, narrow sperm H3K4me3 regions showed little overlapping signal with broad H3K4me3 domains in the oocyte, whereas they overlapped the 2-cell and 8-cell embryo H3K4me3 enrichments (Figures 6A–6F). We identified 20,206 regions in 8-cell embryos that had H3K4me3 enrichment at regions with H3K4me3 in sperm (Figures 6A and 6D).

To elucidate whether diet-altered H3K4me3 regions in sperm were also altered in 8-cell embryos at the same genomic loci, we focused our analysis on ± 1 kb from the center of the regions with altered H3K4me3 in FD WT sperm (= 1,434 regions), and selected regions with detectable H3K4me3 enrichment in the 8-cell embryo (= 922 regions). Of these targeted 922 regions, 494 regions were increased in H3K4me3 in 8-cell embryos from FD WT males, and 428 regions were decreased (Figure S6B). This confirmed that a subset of altered H3K4me3 regions in FD sperm were also altered in the FD WT sired embryos in comparison to those sired by FS WT males. We found 230

Figure 5. Paternally inherited H3K4me3 persists in pre-implantation embryo at regions with H3K4me3 in sperm and at regions with diet-altered H3K4me3 in sperm

(A) Heatmap of total 2-cell embryo H3K4me3 signal (n = 2, data from Liu et al., 2016) ± 3 kb the center of H3K4me3 regions in sperm.

(B–G) Heatmaps of paternal-specific H3K4me3 signal across stages of pre-implantation embryogenesis (n = 2, data from Zhang et al., 2016) at ± 3 kb the center of H3K4me3 regions in sperm. Color of the signal corresponds to relative RPKM counts.

(H and I) Integrative Genome Viewer tracks of re-analyzed datasets from Liu et al. (2016) for 2-cell H3K4me3, and Zhang et al. (2016) for oocyte H3K4me3 and maternal and paternal alleles of PN5 to 4-cell stage embryos. Purple boxes denote maintenance of sperm H3K4me3 (this study) on the embryos' paternal allele at (H) the *Snx13* gene and (I) the *Sdccag8* gene.

(J) Top Venn diagram indicates the number of regions with detectable H3K4me3 in the 2-cell embryos (data from Liu et al., 2016) ± 1 kb the center of H3K4me3 regions in sperm that overlap regions with altered H3K4me3 in FD WT and FD TG sperm. Bottom Venn diagram indicates the number of regions with detectable H3K4me3 on the paternal allele of the PN5 zygote (n = 2, data from Zhang et al., 2016) ± 1 kb the center of H3K4me3 regions in sperm, that overlap regions with altered H3K4me3 in FD WT and FD TG sperm.

(K–N) Heatmaps of FS WT sperm H3K4me3 signal (n = 5 males) (K), sperm CTCF signal (n = 2, data from Jung et al., 2017) (M), and 2-cell H3K4me3 signal (n = 2, data from Liu et al., 2016) (M), and 2-cell H3K4me3 signal (n = 2, data from Liu et al., 2016) (N) ± 3 kb the center of H3K4me3 regions in sperm. Color of the signal corresponds to relative RPKM counts.

(O) Selected significant pathways from gene ontology analysis on the promoters (= 7,170 regions comprising 3,816 promoters) belonging to the top quartile of sorted sperm H3K4me3 regions.

(P) Selected significant pathways from gene ontology analysis on the promoters (= 21,509 regions comprising 9,682 promoters) belonging to the bottom three quartiles of sorted sperm H3K4me3 regions.

Please cite this article in press as: Lismer et al., Histone H3 lysine 4 trimethylation in sperm is transmitted to the embryo and associated with diet-induced phenotypes in the offspring, Developmental Cell (2021), https://doi.org/10.1016/j.devcel.2021.01.014

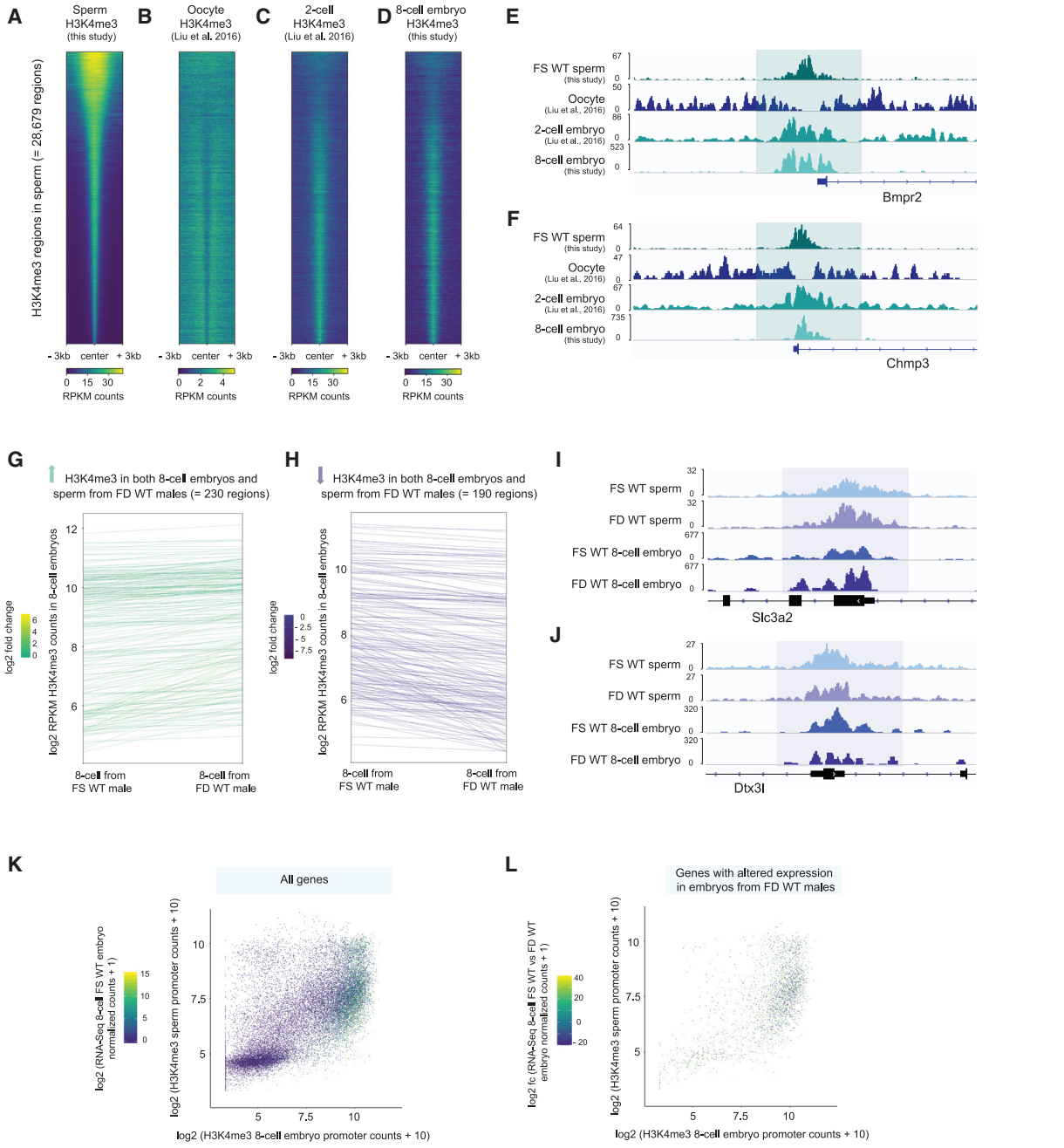

Figure 6. Paternal folate deficiency is linked to altered H3K4 trimethylation profiles in the pre-implantation embryo

Ultra-low-input ChIP-sequencing for H3K4me3 was performed on 8-cell embryos from paternal FS WT C57BL/6J x maternal FS WT C57BL6/J and paternal FD WT C57BL6/J x maternal FS WT C57BL6/J breeding (n = 1–2 replicates with approximately 32 embryos pooled per replicate. 3–4 different males were used for each replicate; Figure S6A).

(A–D) Heatmaps indicating H3K4me3 regions in FS WT sperm (n = 2) (A) and their H3K4me3 enrichment in WT oocytes (n = 2, data from Liu et al., 2016) (B), 2-cell embryos (n = 2, data from Liu et al., 2016) (C), and FS WT 8-cell embryos (n = 2, this study) (D). Color of the signal corresponds to relative RPKM counts.

(E and F) Integrative Viewer Genome tracks of (E) the *Bmpr2* promoter and (F) the *Chmp3* promoter where FS WT sperm signal is mutually exclusive from oocyte H3K4me3 signal (n = 2, data from Liu et al. (2016) but similar to 2-cell (n = 2, data from Liu et al. (2016) and 8-cell embryo H3K4me3 signal (this study).

(G) Line plot indicating regions with increased H3K4me3 in 8-cell embryos from FD WT males at ± 1-kb regions with increased H3K4me3 in FD WT sperm (= 230 regions, $\log_2$ fold change of RPKM normalized counts > 0). Color gradient indicates differential enrichments ($\log_2$ fold change of RPKM normalized counts) between 8-cell embryos from FS WT or FD WT males.

(H) Line plot indicating regions with decreased H3K4me3 in 8-cell embryos from FD WT males at ± 1-kb regions with decreased H3K4me3 in FD WT sperm (= 190 regions, $\log_2$ fold change of RPKM normalized counts < 0). Color gradient indicates differential enrichments ($\log_2$ fold change of RPKM normalized counts) between 8-cell embryos from FS WT or FD WT males.

(I) Integrative Genome Viewer tracks of the *Slc3a2* gene with increased H3K4me3 in FD WT sperm and increased H3K4me3 in 8-cell embryos from FD WT males.

(legend continued on next page)

Please cite this article in press as: Lismer et al., Histone H3 lysine 4 trimethylation in sperm is transmitted to the embryo and associated with diet-induced phenotypes in the offspring, Developmental Cell (2021), https://doi.org/10.1016/j.devcel.2021.01.014

regions with increased H3K4me3 in both 8-cell embryos from FD WT males and FD WT sperm (Figures 6G and 6I). Similarly, 190 regions with decreased H3K4me3 in 8-cell embryos from FD WT males also had decreased H3K4me3 in FD WT sperm (Figures 6H and 6J). Thus, this suggests a partial retention of aberrant H3K4me3 from sperm in the pre-implantation embryo. There were 512 regions with altered H3K4me3 in sperm that had undetectable levels of H3K4me3 in the 8-cell embryo (Figure S6B). In summary, this analysis shows that 64% of the sperm H3K4me3 changes associated with diet were also differentially enriched in the pre-implantation embryo, with about half of these regions conserving the same directionality of enrichment changes from the sperm to the embryo.

To determine how sperm and embryo H3K4me3 were related to embryonic gene expression we selected promoters with high H3K4me3 enrichments in FS WT sperm and embryos from FS WT males (Figures S6C– S6E). Promoters that were highly enriched for H3K4me3 in both sperm and 8-cell embryos, corresponded to highly expressed embryonic genes (hypergeometric test, $p < 0.0001$; Figure 6K). Concordantly, promoters associated with altered gene expression in 8-cell embryos from FD WT males were also enriched for H3K4me3 in sperm and in 8-cell embryos (hypergeometric test, $p < 0.0001$; Figure 6L). Finally, we linked regions with altered H3K4me3 in 8-cell embryos to genes that had altered expression at that stage (Figures S6F–S6I). There were 26% of promoters with altered H3K4me3 in both sperm and 8-cell embryos from FD WT males corresponding to genes expressed in the 8-cell embryo, that significantly overlapped genes with deregulated expression in embryos from FD WT males (Fisher test, $p < 0.0001$; Figure S6F). Promoters that maintained their enrichment directionality changes from sperm to the embryo also significantly overlapped changes in gene expression in 8-cell embryos from FD WT males (Fisher test, $p < 0.05$; Figure S6G).

DISCUSSION

Here, we demonstrate that epigenomic programing at the level of histone methylation is not limited to the period of *in utero* embryo development, indicating that exposures during the lifetime of a mammal can also impact the heritable sperm epigenome. We identified specific regions of sperm chromatin that are sensitive to low dietary folate when exposure began outside embryonic periods of epigenetic reprogramming. Interestingly, regions with abnormal H3K4me3 in FD WT and FD TG sperm closely reflected the birth defects observed in the males' offspring. These phenotypes, which included spinal and craniofacial abnormalities, as well as underdevelopment at birth, are well documented birth defects in FD populations (Benoist, 2008).

Strikingly, 25% of promoters with aberrant H3K4me3 in the sperm of FD WT and FD TG mice that mapped to genes expressed in the 8-cell embryo, overlapped genes with altered gene expression in 8-cell embryos from FD males. The deregulated genes were specific to the 8-cell stage, where the embryo must undergo rapid cell divisions and dramatic chromatin remodeling (Liu et al., 2016). Promoters with altered H3K4me3 in FD sperm may influence gene expression in a time- and tissue-specific manner based on developmental stage. Had we examined more developmental stages, it is possible that we would have discovered more differentially expressed genes that were associated with altered H3K4me3 in sperm. This possibility is supported by the finding that promoters with altered H3K4me3 in FD WT and FD TG sperm also included genes implicated in later developmental events such as organogenesis and post-implantation patterning. The mechanisms by which sperm-inherited chromatin aberrations escape reprogramming and persist throughout embryogenesis remain unknown but is a pressing question for the field of epigenetic inheritance.

During development, enhancers fine tune developmental pathways and drive tissue-specific embryonic gene expression in the embryo (Attanasio et al., 2013; Jadhav et al., 2019). Enhancers regulate gene expression in *cis* and in *trans* and their deletion provokes limb, brain, heart, and craniofacial abnormalities (Attanasio et al., 2013; Osterwalder et al., 2018). In our dataset, we identified an over-representation of tissue-specific putative developmental enhancers in regions with depleted H3K4me3 in FD WT sperm. Enhancers with altered H3K4me3 in FD WT sperm may be decommissioned during early embryogenesis, leading to a reduction in embryonic gene expression at their proximal promoter. Establishing a temporal and spatial network of enhancer-to-promoter interactions during development, will be critical to further understand how the non-canonical distribution of histone modifications in distal regions serve in embryo development, and epigenetic inheritance.

Our study offers insights regarding the involvement of histone H3K4me3 in the transmission of epigenetic information from the sperm to the pre-implantation embryo in mammals. Here, we show that aberrant chromatin from FD sperm maintains abnormalities in the 8-cell embryo. It is worth reminding that by the 8-cell embryo stage, a significant amount of transcription, chromatin remodeling, and DNA methylation reprogramming have occurred (Dahl et al., 2016; Liu et al., 2016; Zhang et al., 2016). This may explain why the directionality changes in H3K4me3 from the sperm to the 8-cell embryo were not fully conserved. We found that regions of narrow H3K4me3 enrichment in sperm that are also present in the 8-cell embryo are mutually exclusive from the broad H3K4me3 domains in the oocyte (Liu et al., 2016). This further implies that sperm H3K4me3 contributes to establishing the embryo's epigenome. We re-analyzed a published dataset (Zhang et al., 2016) and show that paternal H3K4me3 is retained in the PN5 embryo at the same H3K4me3 regions that are altered by the FD diet in sperm. In their study, Zhang et al. normalized their H3K4me3 allele-specific pre-implantation embryo data by calculating the differences of read numbers between both

(J) Integrative Genome Viewer tracks of *Dtx3l* gene with decreased H3K4me3 in FD WT sperm and decreased H3K4me3 in 8-cell embryos from FD WT males. (K and L) Scatterplots where the x axis corresponds to the $\log_2$ (H3K4me3 8-cell embryo from FS WT males promoter counts + 10) and the y axis corresponds to the $\log_2$ (H3K4me3 FS WT sperm promoter counts + 10) at (K) all promoters in the mouse genome, (L) promoters with altered gene expression in 8-cell embryos from FD WT males. Color of the scatter points correspond to the level of gene expression in the 8-cell embryos from FS WT males (K) or $\log_2$ fold change expression between 8-cell embryos from FS WT versus FD WT males (L).

alleles (paternal − maternal) divided by the total number of allelic reads (paternal + maternal). During spermatogenesis, however, a majority of sperm histones are evicted to be replaced by protamines (Balhorn et al., 1977), leading to retention of 1% of histones in mouse sperm. In contrast, the oocytes acquire large H3K4me3 domains throughout oogenesis. The normalization used by Zhang et al. does not take into account these gametic H3K4me3 enrichment imbalances, which consequently artificially reduces the paternal signal in the pre-implantation embryo. Using a reads per kilobase per million mapped (RPKM) normalization on separate paternal and maternal reads allowed us to visualize paternal H3K4me3 signals in the PN5 embryo, at regions with altered H3K4me3 in FD WT and FD TG sperm. Of equal importance, we found that over 58% of PN5 embryo reads that mapped to the mouse genome did not contain a SNP and were, therefore, not included in the analysis. This led to detection of only 6.6 million reads on the paternal allele of the PN5 embryo and likely entails an underestimation of sperm-inherited H3K4me3 in the pre-implantation embryo. To date, drawing conclusions as to whether sperm H3K4me3 is completely inherited or semi-conserved in the PN5 embryo is not possible due to the limitations of SNP-based analyses, as well as low-input chromatin immunoprecipitation techniques, which are unable to efficiently capture regions of low histone enrichment (Brind'Amour et al., 2015; Zhang et al., 2016).

Finally, other factors, such as, non-coding RNA, DNA methylation, DNA binding proteins, and other histone modifications, may act separately or in concert with sperm H3K4me3 to mediate epigenetic inheritance through the paternal germline (Chen et al., 2016; Ly et al., 2017; Sharma et al., 2016). As seen from our transcriptome analysis in 8-cell embryos, multiple chromatin remodeling pathways appear to be affected by the paternal folate deficiency. Additionally, many other histone modifications co-localize with H3K4me3 in sperm (Erkek et al., 2013; Jung et al., 2017; Lismer et al., 2020). Enrichment imbalances between multiple histone modifications in sperm are more likely to drive changes in gene expression in the pre-implantation embryo than an enrichment change of exclusively one histone modification. Taken together, this study indicates that non-genetic inheritance through histone modifications in sperm are intimately involved in offspring development.

STAR★METHODS

Detailed methods are provided in the online version of this paper and include the following:

SUPPLEMENTAL INFORMATION

Supplemental Information can be found online at https://doi.org/10.1016/j.devcel.2021.01.014.

ACKNOWLEDGMENTS

We thank McGill University mouse facility personnel, the Génome Québec Innovation Center, and Kinny Kreiswirth for providing us with a graphical abstract. This research was funded by the Canadian Institute of Health Research (S.K. grant #358654).

AUTHOR CONTRIBUTIONS

S.K. conceived, funded, and guided the project. A.L., C.L., R.L., and V.D. performed the experiments; S.K., A.L., V.D., and R.L., developed the methodology and created the models. J.B.A. and M.C.L. assisted in the methodology of the ULI-ChIP-seq and reviewed and edited the manuscript. A.L. and V.D. performed the analysis and software development; S.K. and A.L. interpreted the findings and wrote the manuscript. Data are available on Gene Expression Omnibus under GEO: GSE135678.

DECLARATION OF INTERESTS

The authors declare no competing interests.

Received: August 20, 2020
Revised: December 1, 2020
Accepted: January 20, 2021
Published: February 16, 2021

REFERENCES

Alexa, A., Rahnenführer, J., and Lengauer, T. (2006). Improved scoring of functional groups from gene expression data by decorrelating GO graph structure. Bioinformatics *22*, 1600–1607.

Aoshima, K., Inoue, E., Sawa, H., and Okada, Y. (2015). Paternal H3K4 methylation is required for minor zygotic gene activation and early mouse embryonic development. EMBO Rep. *16*, 803–812.

Attanasio, C., Nord, A.S., Zhu, Y., Blow, M.J., Li, Z., Liberton, D.K., Morrison, H., Plajzer-Frick, I., Holt, A., Hosseini, R., et al. (2013). Fine tuning of craniofacial morphology by distant-acting enhancers. Science *342*, 1241006.

Bailey, R.L., West, K.P., Jr., and Black, R.E. (2015). The epidemiology of global micronutrient deficiencies. Ann. Nutr. Metab. *66*, 22–33.

Balhorn, R., Gledhill, B.L., and Wyrobek, A.J. (1977). Mouse sperm chromatin proteins: quantitative isolation and partial characterization. Biochemistry *16*, 4074–4080.

Benoist, B. (2008). Conclusions of a WHO Technical Consultation on folate and vitamin B12 deficiencies. Food Nutr. Bull. *29*, S238–S244.

Bolger, A.M., Lohse, M., and Usadel, B. (2014). Trimmomatic: a flexible trimmer for Illumina sequence data. Bioinformatics *30*, 2114–2120.

Brind'Amour, J., Liu, S., Hudson, M., Chen, C., Karimi, M.M., and Lorincz, M.C. (2015). An ultra-low-input native ChIP-seq protocol for genome-wide profiling of rare cell populations. Nat. Commun. *6*, 6033.

Brykczynska, U., Hisano, M., Erkek, S., Ramos, L., Oakeley, E.J., Roloff, T.C., Beisel, C., Schübeler, D., Stadler, M.B., and Peters, A.H. (2010). Repressive and active histone methylation mark distinct promoters in human and mouse spermatozoa. Nat. Struct. Mol. Biol. *17*, 679–687.

Calo, E., and Wysocka, J. (2013). Modification of enhancer chromatin: what, how, and why? Mol. Cell *49*, 825–837.

Carone, B.R., Hung, J.H., Hainer, S.J., Chou, M.T., Carone, D.M., Weng, Z., Fazzio, T.G., and Rando, O.J. (2014). High-resolution mapping of chromatin packaging in mouse embryonic stem cells and sperm. Dev. Cell *30*, 11–22.

Cavalcante, R.G., and Sartor, M.A. (2017). annotatr: genomic regions in context. Bioinformatics *33*, 2381–2383.

Chen, Q., Yan, M., Cao, Z., Li, X., Zhang, Y., Shi, J., Feng, G.H., Peng, H., Zhang, X., Zhang, Y., et al. (2016). Sperm tsRNAs contribute to intergenerational inheritance of an acquired metabolic disorder. Science *351*, 397–400.

Chen, T., and Dent, S.Y. (2014). Chromatin modifiers and remodellers: regulators of cellular differentiation. Nat. Rev. Genet. *15*, 93–106.

Christianson, A., Howson, C.P., and Modell, B. (2006). Executive summary: march of dimes global report on birth defects (March of Dimes). https://www.marchofdimes.org/materials/global-report-on-birth-defects-the-hidden-toll-of-dying-and-disabled-children-executive-summary.pdf.

Conway, J.R., Lex, A., and Gehlenborg, N. (2017). UpSetR: an R package for the visualization of intersecting sets and their properties. Bioinformatics *33*, 2938–2940.

Dahl, J.A., Jung, I., Aanes, H., Greggains, G.D., Manaf, A., Lerdrup, M., Li, G., Kuan, S., Li, B., Lee, A.Y., et al. (2016). Broad histone H3K4me3 domains in mouse oocytes modulate maternal-to-zygotic transition. Nature *537*, 548–552.

Eckersley-Maslin, M.A., Alda-Catalinas, C., and Reik, W. (2018). Dynamics of the epigenetic landscape during the maternal-to-zygotic transition. Nat. Rev. Mol. Cell Biol. *19*, 436–450.

Eisenberg, M.L., Kim, S., Chen, Z., Sundaram, R., Schisterman, E.F., and Buck Louis, G.M. (2014). The relationship between male BMI and waist circumference on semen quality: data from the LIFE study. Hum. Reprod. *29*, 193–200.

Erkek, S., Hisano, M., Liang, C.Y., Gill, M., Murr, R., Dieker, J., Schübeler, D., van der Vlag, J., Stadler, M.B., and Peters, A.H. (2013). Molecular determinants of nucleosome retention at CpG-rich sequences in mouse spermatozoa. Nat. Struct. Mol. Biol. *20*, 868–875.

Haeussler, M., Zweig, A.S., Tyner, C., Speir, M.L., Rosenbloom, K.R., Raney, B.J., Lee, C.M., Lee, B.T., Hinrichs, A.S., Gonzalez, J.N., et al. (2019). The UCSC genome browser database: 2019 update. Nucleic Acids Res. *47*, D853–D858.

Hajkova, P., Ancelin, K., Waldmann, T., Lacoste, N., Lange, U.C., Cesari, F., Lee, C., Almouzni, G., Schneider, R., and Surani, M.A. (2008). Chromatin dynamics during epigenetic reprogramming in the mouse germ line. Nature *452*, 877–881.

Hammoud, S.S., Nix, D.A., Zhang, H., Purwar, J., Carrell, D.T., and Cairns, B.R. (2009). Distinctive chromatin in human sperm packages genes for embryo development. Nature *460*, 473–478.

Hanna, C.W., Taudt, A., Huang, J., Gahurova, L., Kranz, A., Andrews, S., Dean, W., Stewart, A.F., Colomé-Tatché, M., and Kelsey, G. (2018). MLL2 conveys transcription-independent H3K4 trimethylation in oocytes. Nat. Struct. Mol. Biol. *25*, 73–82.

Hanson, M.A., and Skinner, M.K. (2016). Developmental origins of epigenetic transgenerational inheritance. Environ. Epigenet. *2*, dvw002.

Hill, P.W.S., Leitch, H.G., Requena, C.E., Sun, Z., Amouroux, R., Roman-Trufero, M., Borkowska, M., Terragni, J., Vaisvila, R., Linnett, S., et al. (2018). Epigenetic reprogramming enables the transition from primordial germ cell to gonocyte. Nature *555*, 392–396.

Hisano, M., Erkek, S., Dessus-Babus, S., Ramos, L., Stadler, M.B., and Peters, A.H. (2013). Genome-wide chromatin analysis in mature mouse and human spermatozoa. Nat. Protoc. *8*, 2449–2470.

Hyun, K., Jeon, J., Park, K., and Kim, J. (2017). Writing, erasing and reading histone lysine methylations. Exp. Mol. Med. *49*, e324.

Ingrid, L., and Zhaurova, K. (2008). Birth defects: causes and statistics. Nat. Edu. *1*, 18.

Jadhav, U., Cavazza, A., Banerjee, K.K., Xie, H., O'Neill, N.K., Saenz-Vash, V., Herbert, Z., Madha, S., Orkin, S.H., Zhai, H., and Shivdasani, R.A. (2019). Extensive recovery of embryonic enhancer and gene memory stored in hypomethylated enhancer DNA. Mol. Cell *74*, 542–554.e5.

Johnson, M., et al. (1986). Manipulating the Mouse Embryo: A Laboratory Manual (Cold Spring Harbor Laboratory).

Jung, Y.H., Sauria, M.E.G., Lyu, X., Cheema, M.S., Ausio, J., Taylor, J., and Corces, V.G. (2017). Chromatin states in mouse sperm correlate with embryonic and adult regulatory landscapes. Cell Rep. *18*, 1366–1382.

Khoury, A., Achinger-Kawecka, J., Bert, S.A., Smith, G.C., French, H.J., Luu, P.L., Peters, T.J., Du, Q., Parry, A.J., Valdes-Mora, F., et al. (2020). Constitutively bound CTCF sites maintain 3D chromatin architecture and long-range epigenetically regulated domains. Nat. Commun. *11*, 54.

Kim, D., Langmead, B., and Salzberg, S.L. (2015). HISAT: a fast spliced aligner with low memory requirements. Nat. Methods *12*, 357–360.

Kimmins, S., and Sassone-Corsi, P. (2005). Chromatin remodelling and epigenetic features of germ cells. Nature *434*, 583–589.

Knock, E., Deng, L., Wu, Q., Lawrance, A.K., Wang, X.L., and Rozen, R. (2008). Strain differences in mice highlight the role of DNA damage in neoplasia induced by low dietary folate. J. Nutr. *138*, 653–658.

Krueger, F., and Andrews, S.R. (2016). SNPsplit: allele-specific splitting of alignments between genomes with known SNP genotypes. F1000Res. *5*, 1479.

Lambrot, R., Lafleur, C., and Kimmins, S. (2015). The histone demethylase KDM1A is essential for the maintenance and differentiation of spermatogonial stem cells and progenitors. FASEB J. *29*, 4402–4416.

Lambrot, R., Xu, C., Saint-Phar, S., Chountalos, G., Cohen, T., Paquet, M., Suderman, M., Hallett, M., and Kimmins, S. (2013). Low paternal dietary folate alters the mouse sperm epigenome and is associated with negative pregnancy outcomes. Nat. Commun. *4*, 2889.

Langmead, B., and Salzberg, S.L. (2012). Fast gapped-read alignment with Bowtie 2. Nat. Methods *9*, 357–359.

Larose, H., Shami, A.N., Abbott, H., Manske, G., Lei, L., and Hammoud, S.S. (2019). Gametogenesis: a journey from inception to conception. Curr. Top. Dev. Biol. *132*, 257–310.

Lawrence, M., Gentleman, R., and Carey, V. (2009). rtracklayer: an R package for interfacing with genome browsers. Bioinformatics *25*, 1841–1842.

Leek, J.T., Johnson, W.E., Parker, H.S., Jaffe, A.E., and Storey, J.D. (2012). The sva package for removing batch effects and other unwanted variation in high-throughput experiments. Bioinformatics *28*, 882–883.

Lesch, B.J., Silber, S.J., McCarrey, J.R., and Page, D.C. (2016). Parallel evolution of male germline epigenetic poising and somatic development in animals. Nat. Genet. *48*, 888–894.

Li, H., Handsaker, B., Wysoker, A., Fennell, T., Ruan, J., Homer, N., Marth, G., Abecasis, G., and Durbin, R. (2009). The sequence alignment/map format and SAMtools. Bioinformatics *25*, 2078–2079.

Lismer, A., Siklenka, K., Lafleur, C., Dumeaux, V., and Kimmins, S. (2020). Sperm histone H3 lysine 4 trimethylation is altered in a genetic mouse model of transgenerational epigenetic inheritance. Nucleic Acids Res. *48*, 11380–11393.

Liu, X., Wang, C., Liu, W., Li, J., Li, C., Kou, X., Chen, J., Zhao, Y., Gao, H., Wang, H., et al. (2016). Distinct features of H3K4me3 and H3K27me3 chromatin domains in pre-implantation embryos. Nature *537*, 558–562.

Love, M.I., Huber, W., and Anders, S. (2014). Moderated estimation of fold change and dispersion for RNA-seq data with DESeq2. Genome Biol. *15*, 550.

Lun, A.T.L., and Smyth, G.K. (2016). csaw: a bioconductor package for differential binding analysis of ChIP-seq data using sliding windows. Nucleic Acids Res. *44*, e45.

Ly, L., Chan, D., Aarabi, M., Landry, M., Behan, N.A., MacFarlane, A.J., and Trasler, J. (2017). Intergenerational impact of paternal lifetime exposures to both folic acid deficiency and supplementation on reproductive outcomes and imprinted gene methylation. Mol. Hum. Reprod. *23*, 461–477.

Maezawa, S., Yukawa, M., Alavattam, K.G., Barski, A., and Namekawa, S.H. (2018). Dynamic reorganization of open chromatin underlies diverse transcriptomes during spermatogenesis. Nucleic Acids Res. *46*, 593–608.

Osterwalder, M., Barozzi, I., Tissières, V., Fukuda-Yuzawa, Y., Mannion, B.J., Afzal, S.Y., Lee, E.A., Zhu, Y., Plajzer-Frick, I., Pickle, C.S., et al. (2018). Enhancer redundancy provides phenotypic robustness in mammalian development. Nature *554*, 239–243.

Padmanabhan, N., Jia, D., Geary-Joo, C., Wu, X., Ferguson-Smith, A.C., Fung, E., Bieda, M.C., Snyder, F.F., Gravel, R.A., Cross, J.C., and Watson, E.D. (2013). Mutation in folate metabolism causes epigenetic instability and transgenerational effects on development. Cell *155*, 81–93.

Pertea, M., Kim, D., Pertea, G.M., Leek, J.T., and Salzberg, S.L. (2016). Transcript-level expression analysis of RNA-seq experiments with HISAT, StringTie and Ballgown. Nat. Protoc. *11*, 1650–1667.

Phillips, J.E., and Corces, V.G. (2009). CTCF: master weaver of the genome. Cell *137*, 1194–1211.

Radford, E.J., Ito, M., Shi, H., Corish, J.A., Yamazawa, K., Isganaitis, E., Seisenberger, S., Hore, T.A., Reik, W., Erkek, S., et al. (2014). In utero effects. In utero undernourishment perturbs the adult sperm methylome and intergenerational metabolism. Science *345*, 1255903.

Ramírez, F., Ryan, D.P., Grüning, B., Bhardwaj, V., Kilpert, F., Richter, A.S., Heyne, S., Dündar, F., and Manke, T. (2016). deepTools2: a next generation web server for deep-sequencing data analysis. Nucleic Acids Res. *44*, W160–W165.

Reeves, P.G., Nielsen, F.H., and Fahey, G.C., Jr. (1993). AIN-93 purified diets for laboratory rodents: final report of the American institute of nutrition ad hoc writing committee on the reformulation of the AIN-76A rodent diet. J. Nutr. *123*, 1939–1951.

Robinson, M.D., McCarthy, D.J., and Smyth, G.K. (2010). edgeR: a Bioconductor package for differential expression analysis of digital gene expression data. Bioinformatics *26*, 139–140.

Rodgers, A.B., Morgan, C.P., Bronson, S.L., Revello, S., and Bale, T.L. (2013). Paternal stress exposure alters sperm microRNA content and reprograms offspring HPA stress axis regulation. J. Neurosci. *33*, 9003–9012.

Schultz, R.M., Stein, P., and Svoboda, P. (2018). The oocyte-to-embryo transition in mouse: past, present, and future. Biol. Reprod. *99*, 160–174.

Serefidou, M., Venkatasubramani, A.V., and Imhof, A. (2019). The impact of one carbon metabolism on histone methylation. Front. Genet. *10*, 764.

Sharma, U., Conine, C.C., Shea, J.M., Boskovic, A., Derr, A.G., Bing, X.Y., Belleannee, C., Kucukural, A., Serra, R.W., Sun, F., et al. (2016). Biogenesis and function of tRNA fragments during sperm maturation and fertilization in mammals. Science *351*, 391–396.

Shen, Y., Yue, F., McCleary, D.F., Ye, Z., Edsall, L., Kuan, S., Wagner, U., Dixon, J., Lee, L., Lobanenkov, V.V., and Ren, B. (2012). A map of the cis-regulatory sequences in the mouse genome. Nature *488*, 116–120.

Siklenka, K., Erkek, S., Godmann, M., Lambrot, R., McGraw, S., Lafleur, C., Cohen, T., Xia, J., Suderman, M., Hallett, M., et al. (2015). Disruption of histone methylation in developing sperm impairs offspring health transgenerationally. Science *350*, aab2006.

Teperek, M., Simeone, A., Gaggioli, V., Miyamoto, K., Allen, G.E., Erkek, S., Kwon, T., Marcotte, E.M., Zegerman, P., Bradshaw, C.R., et al. (2016). Sperm is epigenetically programmed to regulate gene transcription in embryos. Genome Res. *26*, 1034–1046.

van de Werken, C., van der Heijden, G.W., Eleveld, C., Teeuwssen, M., Albert, M., Baarends, W.M., Laven, J.S.E., Peters, A.H.F.M., and Baart, E.B. (2014). Paternal heterochromatin formation in human embryos is H3K9/HP1 directed and primed by sperm-derived histone modifications. Nat. Commun. *5*, 5868.

Watkins, A.J., Dias, I., Tsuro, H., Allen, D., Emes, R.D., Moreton, J., Wilson, R., Ingram, R.J.M., and Sinclair, K.D. (2018). Paternal diet programs offspring health through sperm- and seminal plasma-specific pathways in mice. Proc. Natl. Acad. Sci. USA *115*, 10064–10069.

Welch, R.P., Lee, C., Imbriano, P.M., Patil, S., Weymouth, T.E., Smith, R.A., Scott, L.J., and Sartor, M.A. (2014). ChIP-enrich: gene set enrichment testing for ChIP-seq data. Nucleic Acids Res. *42*, e105.

Wickham, H. (2016). Ggplot2: Elegant Graphics for Data Analysis (Springer-Verlag).

World Health Organization (2016). Congenital anomalies. https://www.who.int/health-topics/congenital-anomalies#tab=tab_1.

Yamaguchi, K., Hada, M., Fukuda, Y., Inoue, E., Makino, Y., Katou, Y., Shirahige, K., and Okada, Y. (2018). Re-evaluating the localization of sperm-retained histones revealed the modification-dependent accumulation in specific genome regions. Cell Rep. *23*, 3920–3932.

Yang, J., Carmichael, S.L., Canfield, M., Song, J., and Shaw, G.M.; National Birth Defects Prevention Study (2008). Socioeconomic status in relation to selected birth defects in a large multicentered US case-control study. Am. J. Epidemiol. *167*, 145–154.

Zhang, B., Zheng, H., Huang, B., Li, W., Xiang, Y., Peng, X., Ming, J., Wu, X., Zhang, Y., Xu, Q., et al. (2016). Allelic reprogramming of the histone modification H3K4me3 in early mammalian development. Nature *537*, 553–557.

Please cite this article in press as: Lismer et al., Histone H3 lysine 4 trimethylation in sperm is transmitted to the embryo and associated with diet-induced phenotypes in the offspring, Developmental Cell (2021), https://doi.org/10.1016/j.devcel.2021.01.014

STAR★METHODS

KEY RESOURCES TABLE

REAGENT or RESOURCE	SOURCE	IDENTIFIER
Antibodies		
Rabbit monoclonal anti-histone 3 lysine 4 trimethylation	Cell Signaling Technology	Cat#9751; RRID:AB_2616028
Rabbit polyclonal anti-histone 3 lysine 4 trimethylation	Diagenode	Cat#C15410003; RRID:AB_2616052
Chemicals, Peptides, and Recombinant Proteins		
Alcian Blue	Sigma Aldrich	Cat#A3157
Alizarin Red	Sigma Aldrich	Cat#A5533
Micrococcal Nuclease (Nuclease S7) used for sperm ChIP-Seq	Roche	Cat#10107921001
Complete Protease Inhibitor Cocktail	Roche	Cat#4693116001
Dithiothreitol	Bio Shop	Cat#3483-12-3
RNAse A	Sigma Aldrich	Cat#10109169001
Proteinase K	Sigma Aldrich	Cat#P2308
Folligon PMSG	CDMV	Cat#103476
hCG	EMD Millipore	Cat#230734
Penicillin-Streptomycin	Thermo Fisher	Cat#15140122
Acidic Tyrode's Solution	Millipore Sigma	Cat#T1788
Micrococcal Nuclease used for 8-cell embryo ULI-ChIP	New England BioLabs	Cat#M0247S
TriReagent	Millipore Sigma	Cat#93289
Phenol:Chloroform	Sigma Aldrich	Cat#77617
Chloroform	Sigma Aldrich	Cat#288306
Elution Buffer	Qiagen	Cat#1014609
Critical Commercial Assays		
40 μM micro-pore filter	Fisher Scientific	Cat#22363547
Protein A Dynabeads	Thermo Fisher	Cat#10002D
Protein G Dynabeads	Thermo Fisher	Cat#10003D
Zymo Kit ChIP DNA Clean and Concentrator	Zymo Research	Cat#D5201
Qiagen Ultralow Input Library Kit	Qiagen	Cat#180495
Agencourt AMPure XP beads	Beckman Coulter	Cat#A63880
M2 Medium	Millipore Sigma	Cat#MR-015-D
Nuclear Isolation Buffer	Sigma Aldrich	Cat#NUC-101
DNA/RNA Protection Reagent	New England Biolabs	Cat#T2011L
NEBNext Single Cell / Low Input RNA Library Preparation Kit	New England BioLabs	Cat#E6420S
Deposited Data		
Mouse sperm H3K4me3	This study	GEO: GSE135678
Mouse 8-cell embryo H3K4me3	This study	GEO: GSE135678
Mouse 8-cell embryo mRNA-Seq	This study	GEO: GSE135678
Mouse sperm H3K4me3 ChIP-Seq 2	Jung et al. 2017	GEO: GSE79230
Mouse sperm H3K4me3 ChIP-Seq 3	Zhang et al., 2016	GEO: GSE71434
Mouse sperm H3K4me3 ChIP-Seq 4	Erkek et al., 2013	GEO: GSE19892
Mouse sperm cohesin and CTCF ChIP-Seq	Jung et al., 2017	GEO: GSE79230

(*Continued on next page*)

Please cite this article in press as: Lismer et al., Histone H3 lysine 4 trimethylation in sperm is transmitted to the embryo and associated with diet-induced phenotypes in the offspring, Developmental Cell (2021), https://doi.org/10.1016/j.devcel.2021.01.014

Continued

REAGENT or RESOURCE	SOURCE	IDENTIFIER
Mouse oocyte and 2-cell embryo H3K4me3 ChIP-Seq	Liu et al., 2016	GEO: GSE73952
Mouse pre-implantation embryo stages (with paternal and maternal reads) H3K4me3 ChIP-Seq	Zhang et al., 2016	GEO: GSE71434
Putative enhancer annotations	Shen et al., 2012	GEO: GSE29184
Experimental Models: Organisms/Strains		
C57BL6/J wildtype male and female mice	Charles River Laboratories	N/A
Germ-cell-specific KDM1A overexpressing TG male mice on a C57BL6/J background	Siklenka et al., 2015	N/A
Software and Algorithms		
Trimmomatic v0.38	Bolger et al., 2014	http://www.usadellab.org/cms/?page=trimmomatic
Bowtie2 v2.3.5	Langmead and Salzberg, 2012	http://bowtie-bio.sourceforge.net/bowtie2/index.shtml
SAMtools v1.7	Li et al., 2009	http://www.htslib.org
Hisat2 v2.1.0	Kim et al., 2015	https://daehwankimlab.github.io/hisat2/
Stringtie v2.0.4	Pertea et al., 2016	https://ccb.jhu.edu/software/stringtie/
DeepTools v3.3.1	Ramírez et al., 2016	https://deeptools.readthedocs.io/en/develop/content/installation.html
annotatr v1.8.0	Cavalcante and Sartor, 2017	http://bioconductor.org/packages/release/bioc/html/annotatr.html
ggplot2 v3.3.2	Wickham, 2016	https://ggplot2.tidyverse.org
chipenrich v2.6.1	Welch et al., 2014	https://www.bioconductor.org/packages/release/bioc/html/chipenrich.html
SNPsplit v0.3.2	Krueger and Andrews, 2016	https://www.bioinformatics.babraham.ac.uk/projects/SNPsplit/
csaw v1.24.3	Lun and Smyth, 2016	https://www.bioconductor.org/packages/release/bioc/html/csaw.html
edgeR v3.24.3	Robinson et al., 2010	http://bioconductor.org/packages/release/bioc/html/edgeR.html
DESeq2 v1.22.2	Love et al., 2014	http://bioconductor.org/packages/release/bioc/html/DESeq2.html
rtracklayer v1.42.2	Lawrence et al., 2009	https://bioconductor.org/packages/release/bioc/html/rtracklayer.html
sva v3.30.1	Leek et al., 2012	https://www.bioconductor.org/packages/release/bioc/html/sva.html
TopGO v2.34.0	Alexa et al., 2006	https://bioconductor.org/packages/release/bioc/html/topGO.html
UpSetR v1.4.0	Conway et al., 2017	https://cran.r-project.org/web/packages/UpSetR/index.html
Other		
Folate Sufficient Mouse Chow	Harlan Laboratories	TD.01369
Folate Deficient Mouse Chow	Harlan Laboratories	TD.01546

RESOURCE AVAILABILITY

Lead contact

Further information and requests for resources and reagents should be directed to and will be fulfilled by the Lead Contact, Sarah Kimmins (sarah.kimmins@mcgill.ca).

Materials availability

This study did not generate new unique reagents.

Data and code availability

The accession number for sperm H3K4me3 ChIP-Seq, 8-cell embryo H3K4me3 ULI-ChIP-Seq, and 8-cell embryo mRNA-Seq data reported in this paper is GEO: GSE135678 (accessible through: https://www.ncbi.nlm.nih.gov/geo/query/acc.cgi?acc=GSE135678).

EXPERIMENTAL MODEL AND SUBJECT DETAILS

Animals

Mice were housed under a controlled light/dark cycle and were provided with food and water *ad libitum*. All animal procedures were approved by the Animal Care and Use Committee of McGill University, Montreal, Canada. The KDM1A transgenic line on a C57BL6/J background was generated in Siklenka et al. (2015). These males were conceived via the microinjection of a human KDM1A construct whose expression is driven by the testes-specific truncated EF1a promoter. Of note, KDM1A TG males are heterozygous. To maintain the line, TG male founders were bred to C57BL/6J females which yielded generation 1 (F1) TG offspring. The phenotype in KDM1A TG offspring observed here was subtler than in Siklenka et al. (2015), as this study was performed using F10 TG males. To keep the TG lines we have to select for survivability (i.e., the least affected offspring) which has led to a dilution of the severity of the phenotype in later generations. All wildtype mice used were also on a C57BL6/J background (Charles Rivers Laboratories).

METHODS DETAILS

Dietary treatments and animal breeding

Dietary treatments for ChIP-Sequencing on sperm

Dietary exposures in male mice began at 3 weeks of age. Male C57BL/6 mice (WT, Charles River Laboratories, St-Constant, QC, Canada) or KDM1A transgenic mice (TG) were fed a folate sufficient (FS, 2.0 mg folic acid per kg, TD.01369, Harlan Laboratories, Madison, WI) or folate deficient (FD, 0.3 mg folic acid per kg, TD.01546) diet for 11 weeks prior to sacrifice and sperm collection. Folate contents were based on previous models (Knock et al., 2008) where the FS diet corresponds to the recommended amount of folic acid for rodents (Reeves et al., 1993) and the FD diet contains about 14.3% of the amount of folic acid of the FS diet.

Dietary treatments for E2.5 breeding

WT female mice were fed a FS or FD diet for 3 weeks beginning at weaning. Females in diestrus phase were superstimulated using 5 IU of PMSG (Folligon, CDMV, #103476). 48 hours after, females were superovulated using 5 IU of hCG (EMD Millipore, #230734) and bred to WT or TG males that had been on an FS or FD diet for 9 – 11 weeks. Per group, 3 – 7 males were used and 3 – 9 litters were generated. Copulation was detected by vaginal plug the next morning and a plug was defined as day E0.5 of pregnancy.

Dietary treatments for E18.5 breeding

WT or TG males fed a FS or FD diet for 9 – 11 weeks were bred to WT females on a regular Chow diet. Per group, 3 – 6 males were used and 7 – 13 litters were generated. Copulation was detected by vaginal plug the next morning and plug a was defined as day E0.5 of pregnancy. On day E18.5, females were sacrificed and the pregnancy outcomes were analyzed. Pre-implantation losses were determined by counting the total number of corpus luteum in the ovary minus the total number of E18.5 embryos in the litter and post-implantation losses as the total number of resorbed sites.

Skeletal staining

One female and one male pup were randomly selected per E18.5 litter for skeletal staining analysis. Skeletal staining was performed according to the Hogan et al. method (Johnson et al., 1986). Briefly, E18.5 carcasses were skinned and eviscerated before overnight fixation in 95% ethanol (EtOH). The carcasses were then stained overnight in Alcian blue solution (Sigma Aldrich, #A3157) then returned to 95% EtOH for 2 to 5 hours. Then, the skeletons were cleared with 2% KOH solution for 24 to 36 hours. After sufficient tissue disintegration, the skeletons were stained overnight in 1% KOH/0.015% Alizarin red solution (Sigma Aldrich, #A5533). Subsequently, skeletons were cleared in 1% KOH/20% glycerol for approximately 48 hours. The stained skeletons were transferred to 50% glycerol / 50% ethanol as storage medium and in preparation for skeletal analysis. Skeletal analysis was performed blind. Skeletal abnormalities were partitioned into mild, moderate and severe abnormalities based on their consequences on pup survivability. 12 fetuses from FS WT males, 18 from FS TG males, 19 from FD WT males, and 32 from FD TG males, were analyzed.

Sperm collection

Sperm was collected from the caudal epididymis using a previously described swim-out procedure (Hisano et al., 2013). Briefly, cauda epididymides were placed into phosphate-buffered saline (PBS), cut, and gently agitated to at 37°C to allow sperm to swim out. The spermatozoa were passed through a 40 μM micro-pore filter (Fisher Scientific, #22363547) to remove somatic cells. Spermatozoa were washed once in PBS and put in freezing medium before being placed in a -80°C freezer.

ChIP-Sequencing on sperm and library preparation

The H3K4me3 ChIP-Sequencing procedure was based on a published method (Hisano et al., 2013), with slight modifications to minimize sample loss and perform the experiment on a single mouse. Briefly, 9 x 10^6 mouse spermatozoa from individual mice were washed three times in PBS and treated with dithiothreitol (Bio Shop, #3483-12-3) to open the chromatin. Mouse spermatozoa were lysed, washed with PBS, and aliquoted into three tubes per sample. Spermatozoa were lysed again and subject to MNase

digestion (Roche, #10107921001) using 15 units per tube for 5 minutes. Reaction was stopped by adding EDTA. After spinning at maximum speed for 10 minutes, supernatants were pooled on ice. Samples were pre-cleared and incubated overnight with 5 μg of H3K4me3 antibody (Cell Signaling, #9751). The next day, samples were washed, eluted, and treated with RNase A (Sigma Aldrich, #10109169001) and Proteinase K (Sigma Aldrich, #P2308). DNA was extracted with the Zymo Kit ChIP DNA Clean and Concentrator (Zymo Research, #D5201). Libraries were prepared using the Qiagen Ultralow Input Library Kit (Qiagen, #180495) as per manufacturer's recommendations. Mononucleosomes were size selected with Agencourt AMPure XP Beads (Beckman Coulter, #A63880) and samples were sequenced using single-end 50 base pair reads with the Illumina HiSeq 4000 SR50 platform (n = 5 individual males per group).

8-cell embryo collection

On embryonic day E2.5, females were sacrificed and their uterus was retrieved. Uterine horns were flushed through the infundibulum using M2 media (Millipore Sigma, #MR-015-D) supplemented with 10% Penicillin-Streptomycin (Thermo Fisher, #15140122), and embryos were collected. For low-input RNA-Seq, 8-cell embryos were washed in drops of M2/PS media and flash frozen in DNA/RNA protection reagent (New England Biolabs, #T2011L). For ULI-ChIP-Seq, 8-cell embryos were washed in drops of M2/PS media and passed through drops of Acidic Tyrode's (Millipore Sigma, #T1788) to remove their zona pellucida. Embryos were washed again in drops of M2/PS media and flash frozen in nuclear isolation buffer (Sigma Aldrich, #NUC-101).

Low-Input mRNA-Sequencing and library preparation on 8-cell embryos

8-cell embryos were thawed on ice and 8-cell embryos from the same male were pooled to obtain approximately 112 cells per replicate. To minimize biases arising from pooling a different number of females together, embryos from 1 female were used per group except for the FD_TG_3 replicate where 2 females had to be pooled to obtain sufficient starting material. Total RNA was extracted using Tri-Reagent (Millipore Sigma, #93289) and mRNA-Seq libraries were generated using the NEBNext Single Cell / Low Input RNA Library Preparation Kit for Illumina (New England Biolabs, #E6420S) using manufacturer recommendations. mRNA was sequenced using paired-end 100 bp sequencing reads with the Illumina HiSeq 4000 PE100 platform (n = 3 replicates per group with approximatively 14 embryos pooled per replicate. A different male was used for each replicate).

Ultra-Low-Input ChIP-Sequencing and library preparation on 8-cell embryos

Ultra-Low-Input ChIP-Sequencing was performed as previously described with slight modifications(Brind'Amour et al., 2015). Embryos in nuclear isolation buffer were thawed on ice and embryos from the same breeding groups were pooled to obtain about 250 cells per immunoprecipitation (2 – 3 litters pooled per ChIP). Cells were lysed and MNase digestion (New England Biolabs, #M0247S) was performed for 7.5 minutes at 21°C. Reaction was stopped by adding EDTA. Chromatin was pre-cleared for an hour and 0.125 μg of H3K4me3 antibody (Diagenode, #C15410003-10) was added based on previous reports indicating optimal antibody concentration for H3K4me3 on 250 cells (Hanna et al., 2018). Samples were pre-cleared and incubated overnight with the antibody. The next day, the samples were washed and DNA was eluted. RNase A (Sigma Aldrich, #10109169001) and Proteinase K (Sigma Aldrich, #P2308) treatments were performed. A phenol:chloroform (Sigma Aldrich, #77617) extraction was done, followed by a chloroform (Sigma Aldrich, #288306) extraction to remove any remnant traces of phenol. DNA was precipitated, pelleted and resuspended in elution buffer (Qiagen, #1014609). Samples were subject to library preparation using the Qiagen Ultra-Low Input Library Kit (Qiagen, #180495) as per manufacturer's recommendations. Mononucleosomes were size selected with Agencourt AMPure XP Beads (Beckman Coulter, #A63880) and samples were sequenced using paired-end 100 base pair reads with the Illumina HiSeq 4000 PE100 platform (n = 1 – 2 per group with approximatively 32 embryos pooled per replicate. 3 – 4 different males were used for each replicate).

Pre-processing

Read statistics for ChIP-Seq data on sperm and 8-cell embryos as well as mRNA-Seq data on 8-cell embryos generated in this study are indicated in Table 1.

Sperm ChIP-Sequencing data

For sperm H3K4me3 datasets from this study, reads were trimmed using Trimmomatic in single-end mode (version 0.38) (Bolger et al., 2014) (TruSeq3-SE.fa:1:30:15 TRAILING:25 MINLEN:30). Reads were mapped to the December 2011 assembly of the mouse genome downloaded from UCSC Genome Browser (mm10, NCBI Build 38) (Haeussler et al., 2019) with Bowtie2 (version 2.3.5) (Langmead and Salzberg, 2012) in single-end mode using the standard settings. SAMtools (version 1.7) (Li et al., 2009) was then used to sort and convert SAM files into BAM files.

8-cell embryo mRNA-Sequencing data

Reads were trimmed using Trimmomatic (version 0.38) (Bolger et al., 2014) in paired-end mode (TruSeq3-PE.fa:1:30:15 TRAILING:25 MINLEN:30). Reads were mapped to the mm10 genome with Hisat2 (version 2.1.0) (Kim et al., 2015) in paired-end mode using the standard settings. SAMtools (version 1.7) (Li et al., 2009) was then used to sort and convert SAM files into BAM files. Transcripts were called using Stringtie (version 2.0.4) (Pertea et al., 2016).

8-cell embryo ULI-ChIP-Sequencing data

Reads were trimmed using Trimmomatic (version 0.38) (Bolger et al., 2014) in paired-end mode (TruSeq3-PE.fa:1:30:15 TRAILING:25 MINLEN:30). Reads were mapped to the mm10 genome with Bowtie2 (version 2.3.5) (Langmead and Salzberg, 2012) in paired-end mode using the standard settings. SAMtools (version 1.7) (Li et al., 2009) was then used to sort and convert SAM files into BAM files.

Please cite this article in press as: Lismer et al., Histone H3 lysine 4 trimethylation in sperm is transmitted to the embryo and associated with diet-induced phenotypes in the offspring, Developmental Cell (2021), https://doi.org/10.1016/j.devcel.2021.01.014

Bigwig coverage tracks

Bigwig coverage tracks were generated from aligned reads using DeepTools2 (version 3.3.1) (Ramírez et al., 2016). The coverage was calculated as the number of reads per 10-bp bins across the genome and normalized using Reads Per Kilobase per Million mapped reads (RPKM).

Paternal allele embryo ChIP-Sequencing data preprocessing

Raw reads for H3K4me3 ChIP-Seq datasets on different stages of pre-implantation embryo development were retrieved from GEO: GSE71434 (Zhang et al., 2016). An N-masked reference genome was generated using PWK/PhJ SNP information for the mm10 mouse genome. Reads were aligned using the Zhang et al. parameters with Bowtie2 (version 2.3.5) (Langmead and Salzberg, 2012). SAMtools (version 1.7) (Li et al., 2009) was then used to sort and convert SAM files into BAM files. SNPsplit (version 0.3.2) (Krueger and Andrews, 2016) was used to identify allele specific reads between paternal (PWK/PhJ genome) and maternal (C57BL/6N genome) alleles. Bigwig coverage tracks for paternal reads and maternal reads were generated and RPKM normalized separately, as described above (version 3.1.1) (Ramírez et al., 2016).

Other used publicly available ChIP-Sequencing datasets

Raw reads from various studies were retrieved from the following accession number: CTCF sperm ChIP-Seq data from Jung et al. (2017) GEO: GSE79230, cohesin sperm ChIP-Seq data from Jung et al. (2017) GEO: GSE79230, H3K4me3 sperm ChIP-Seq data from Zhang et al. (2016) GEO: GSE71434, H3K4me3 sperm ChIP-Seq data from Jung et al. (2017) GEO: GSE79230, H3K4me3 sperm ChIP-Seq data Erkek et al. (2013) GEO: GSE19892, H3K4me3 2-cell embryo ChIP-Seq data from Liu et al. (2016) GEO: GSE73952, H3K4me3 oocyte ChIP-Seq data from Liu et al. (2016) GEO: GSE71434. Reads were trimmed and aligned to the mm10 genome as described above in single-end or paired-end mode accordingly.

QUANTIFICATION AND STATISTICAL ANALYSIS

Bioinformatics analysis

For all bioinformatics analysis, R (version 4.0) was used.

Sperm ChIP-Sequencing data

Sperm H3K4me3 region selection and normalization

Read filtering and normalizations were done with the Bioconductor package csaw (version 1.24.3) (Lun and Smyth, 2016). 150 bp sliding windows were used to count reads in each library genome wide (= 47,762,959 windows). Reads were then counted with contiguous 2000-bp bins across the genome (= 1,282,451 bins). Global background coverage estimated by bin counts were compared to the window-based abundances and background windows were filtered based on a $\log_2$ fold change of 6 over the level of non-specific enrichment (= 765,958 filtered windows). The filtered windows were normalized by library size using counts per million (CPM) normalization, composition bias using trimmed means of M-values (TMM) normalization, and batch effects using the sva ComBat function (version 3.30.1) (Leek et al., 2012). Filtered windows less than 100 bp apart were merged and a maximum peak size of 5,000 bp was permitted, conferring a total of 28,679 regions.

Identification of regions with altered H3K4me3 in sperm

PCA plots were generated on normalized merged regions. The top 5% of regions contributing to principle component 1 (the dietary and genotype effects) were selected and H3K4me3 directionality changes were determined by defining positive and negative $\log_2$ fold changes from the median of normalized counts for each region of the compared groups.

Annotations and Z-Score analyses

Tissue specific enhancer regions were downloaded from ENCODE (GEO: GSE29184) (Shen et al., 2012). Enhancer data was lifted over from mm9 to mm10 using the rtracklayer liftOver function (version 1.42.2) (Lawrence et al., 2009) and enhancer regions were defined as +/- 500 bp around the given center. Craniofacial enhancers were retrieved from Attanasio et al. (2013) and lifted over from mm9 to mm10. For all annotation classes, Z-Score analyses were performed using 1,000 permutation tests. Only significant positive and negative enrichments ($p < 0.05$) are shown.

8-cell embryo mRNA-Sequencing data

Identification of differentially expressed genes in 8-cell embryos from WT or TG males fed a FS or FD diet was done using DESeq2 with a FDR < 0.1 (version 1.22.2) (Love et al., 2014). Transcripts with read counts below 10 were filtered out which conferred 38,263 expressed transcripts in the 8-cell embryo. For data visualization, transcript counts were normalized using the DESeq2 vsd stabilization function and sva ComBat function for batch adjustment (version 3.30.1) (Leek et al., 2012).

To test for trend in transcript expression across the experimental groups (Figures 4F–4I), we assigned numerical values to each group (FS WT = 1; FS TG = 2; FD WT = 2; FD TG = 3) and fit the transcripts with altered gene expression in 8-cell embryos from FD TG males to a linear model as implemented in DESeq2 (version 1.22.2) (Love et al., 2014).

To visualize the trend of expression summarized over all transcripts, we map expression data to a linear order and compute the average rank of transcript expression in each sample. When transcripts had different directionality (as in Figure 4A), we first partitioned transcripts into 2 groups around meloids (M1 and M2) using correlation as the distance metric. In a univariate fashion, each M1 transcript is used to rank n samples from the lowest to the highest expression and expression values of each gene are then replaced by (1,...,n) ranks. M2 transcripts are ordered from the highest to lowest expression and ranks are assigned similarly.

Please cite this article in press as: Lismer et al., Histone H3 lysine 4 trimethylation in sperm is transmitted to the embryo and associated with diet-induced phenotypes in the offspring, Developmental Cell (2021), https://doi.org/10.1016/j.devcel.2021.01.014

This way, the sample, for example in Figure 4A, with the highest mean rank has the highest expression of increased (M1) transcripts in FD WT and the lowest expression of decreased (M2) transcripts in FD WT compared with FS WT.

Paternal allele embryo ChIP-Sequencing

Identification of regions with H3K4me3 enrichment on the paternal allele of the PN5 embryo was done via K-means clustering of heatmap H3K4me3 intensity signal using DeepTools2 (version 3.1.1) (Ramírez et al., 2016).

2-cell embryo and 8-cell embryo ULI-ChIP-Sequencing data

Read counts of 2-cell embryos (data from Liu et al., 2016 and 8-cell embryos (data from this study) were performed +/- 1 kb the center of H3K4me3 regions in sperm and regions with low read counts were filtered out using the edgeR function filterByExpr (version 3.24.3) (Robinson et al., 2010).

Other Bioconductor R packages used

Pearson correlation plot, profile plots and heatmaps were generated using DeepTools2 (version 3.1.1) (Ramírez et al., 2016). Distance to transcriptional start site was determined with chipenrich (version 2.6.1) (Welch et al., 2014). Gene ontology analysis was performed on promoters defined by annotatr (version 1.8.0) (Cavalcante and Sartor, 2017) using TopGO (version 2.34.0) (Alexa et al., 2006). Upset plots were generated with UpSetR (version 1.4.0) (Conway et al., 2017). All other plots were done with ggplot2 (version 3.3.2) (Wickham, 2016).

Statistical analyses for E18.5 pregnancy outcomes

The level of significance for all statistical tests used was set at $p < 0.05$. Pre-implantation and post-implantation variability losses were tested for significance using F-test with Holm-Bonferroni correction. Total number of abnormalities and total number of severe abnormalities were tested for significance using Mann-Whitney's U-test with Holm-Bonferroni correction. Total number of abnormal 8-cell embryos were tested for significance using student-t-test with Holm-Bonferroni correction.